energies

MDPI

Article

Evaluation of Model Predictions of the Unsteady Tidal Stream Resource and Turbine Fatigue Loads Relative to Multi-Point Flow Measurements at Raz Blanchard

Hannah Mullings [1,*], Samuel Draycott [1], Jérôme Thiébot [2], Sylvain Guillou [2], Philippe Mercier [2], Jon Hardwick [3], Ed Mackay [3], Philipp Thies [3] and Tim Stallard [1]

1 School of Engineering, The University of Manchester, Manchester M13 9PL, UK
2 Laboratoire Universitaire de Sciences Appliquées de Cherbourg (LUSAC), University of Caen Normandy (UNICAEN), 50130 Cherbourg en Cotentin, France
3 Renewable Energy Group, College of Engineering, Mathematics and Physical Sciences, University of Exeter, Penryn Campus, Penryn TR10 9FE, UK
* Correspondence: hannah.mullings@manchester.ac.uk

Abstract: The next stage of development of the tidal stream industry will see a focus on the deployment of tidal turbines in arrays of increasing device numbers and rated power. Successful array development requires a thorough understanding of the resource within potential deployment sites. This is predictable in terms of flow speeds, based upon tidal constituents. However, the operating environment for the turbine is more complex than the turbine experiencing a uniform flow, with turbulence, shear and wave conditions all affecting the loading on the turbine components. This study establishes the accuracy with which several alternative modelling tools predict the resource characteristics which define unsteady loading—velocity shear, turbulence and waves—and assesses the impact of the model choice on predicted damage equivalent loads. In addition, the predictions of turbulence are compared to a higher fidelity model and the occurrence of flow speeds to a Delft3D model for currents and waves. These models have been run for a specific tidal site, the Raz Blanchard, one of the major tidal stream sites in European waters. The measured resource and predicted loading are established using data collected in a recent deployment of acoustic Doppler current profilers (ADCPs) as part of the Interreg TIGER project. The conditions are measured at three locations across the site, with transverse spacing of 145.7 m and 59.3 m between each device. Turbine fatigue loading is assessed using measurements and model predictions based on an unsteady blade element momentum model applied to near-surface and near-bed deployment positions. As well as across-site spatial variation of loading, the through life loading over a 5-year period results in an 8% difference to measured loads for a near-surface turbine, using conditions purely defined from a resource model and to within 3% when using a combination of modelled shear with measured turbulence characteristics.

Keywords: tidal turbine; fatigue loading; turbulence, multi-point measurements

Citation: Mullings, H.; Draycott, S.; Thiebot, J.; Guillou, S.; Mercier, P.; Hardwick, J.; Mackay, E.; Thies, P.; Stallard, T. Evaluation of Model Predictions of the Unsteady Tidal Stream Resource and Turbine Fatigue Loads Relative to Multi-Point Flow Measurements at Raz Blanchard. *Energies* **2023**, *16*, 7057. https://doi.org/10.3390/en16207057

Academic Editor: Davide Astolfi

Received: 31 July 2023
Revised: 22 September 2023
Accepted: 29 September 2023
Published: 12 October 2023

1. Introduction

In order to plan for tidal array development, a thorough understanding of the resource is required. Due to the nature of tidal flows, there is high potential for reliable power generation since tidal cycles are highly predictable. This predictability can be defined using tidal constituents which are area-specific in terms of amplitude, but consistent in frequency. Understanding the tides in a specific area allows for a straightforward identification of the most energetic sites that are suitable for tidal stream energy extraction. The deployment of tidal stream turbines, to utilise the reliable tidal resource around the UK, has been shown to offer the potential to supply up to 11% of the UK's electricity demand [1]. This is based upon a review of site assessments of locations around the UK using hydrodynamic resource models. The focus of such site assessments is to examine the potential energy yield and power capture, with limited consideration placed upon the unsteady operating conditions.

A key consideration for tidal turbine developers is establishing the fatigue loads and this requires understanding the onset flow conditions. Various computational models are available for calculating a load time history from which fatigue loads may be obtained, such models range in complexity from fully blade-resolved methods [2,3], to the actuator line method [4,5], actuator disks [6], and blade element momentum theory (BEM) [7–10]. All of these models require the definition of an unsteady onset flow field, which requires a mean velocity ($\overline{u}$), a measure of conditions that induce loads at defined frequencies such as steady shear ($\tilde{u}$), which causes periodic loads at the turbine frequency and waves ($\tilde{u_w}$) resulting in loading at the wave frequency and harmonics, as well as any stochastic fluctuations in the flow caused by turbulence (u'). These elements of the flow field can be determined and created in different ways with the turbulence mainly being synthesised using different computational methods, ranging from computational fluid dynamics (CFD) software of varying complexity to statistical turbulence models. In this paper, the focus is on how those variables differ around a site and how they can be predicted.

This study aims to establish the spatial variation of the unsteady conditions that define operating loads on a typical tidal turbine, the impact of these conditions on fatigue loads and the accuracy with which these flows and loads may be predicted using established modelling techniques. This is assessed using a unique set of three current ADCP measurements, predictions from four resource models and considering multiple turbine locations. Two vertical turbine positions are considered, which are indicative of the hub-height of bed-supported or surface-supported systems, and the long-term through-life loading on the blade calculated for a full range of operating conditions.

The approach builds upon a preliminary study of the variation of shear and turbulence at a tidal site which was conducted by Mullings et al. [11], for the European Marine Energy Centre (EMEC) test site using data from the ReDAPT project. This study focused on the variation at two locations at a site and with comparison between modelled and measured data. However, the modelled data available were limited to the vertical velocity shear and lacked detail on the modelled turbulence parameters. This work continues to explore modelled site characteristics and compares with measured data, establishing the impact on turbine loading between the different input datasets. There are a number of different sites under consideration for tidal stream turbine deployments in the UK–France channel region, from different locations in a site through to different vertical positions, the latter being of key importance to turbine developers focusing on floating or bed-mounted devices.

This study is focused on understanding the conditions at the tidal site Raz Blanchard, a site which has been the subject of numerous measurement campaigns in recent years due to the highly energetic tidal conditions. The data from these measurement campaigns has underpinned various analyses such as those of the characterisation of turbulence [12,13], the spatial variation of conditions [14–16], the change in bathymetry and different bed structures on the flow field [17,18], and the complex wave-current conditions through 3D modelling [19,20]. In most of the foregoing studies, computational resource models have been used in conjunction with measurement data to support analysis. Data from several of these models are used in this work [16,17,20] to provide site characteristics with different levels of computational cost and fidelity, with more detail on these models provided in [21]. Our analysis also draws upon new data from the site obtained from a measurement campaign conducted in 2021–2022, as part of the Interreg TIGER project. This campaign was developed partly to inform understanding of the spatial variability at a tidal site, using multiple devices deployed and measured over a concurrent time span.

This study is split into two sets of analysis, with the first objective establishing the parameters important for an inflow model as input to a loading model. The measured and modelled conditions and their occurrence at different positions in a site also provide spatial variation. These conditions are used as input to an efficient unsteady BEMT model, which was previously validated against experiments [10,22], but could also be used as inflow for other models to determine turbine loading. The second objective was to use the spatially varying conditions to determine the influence of inflow conditions on the turbine loading.

2. Site Focus

Six tidal sites were identified within the Interreg TIGER project within the UK–France channel region with the potential for Tidal stream device deployments. Within the project, a series of eight acoustic Doppler current profilers (ADCPs) were deployed at these sites with the aim of supporting ongoing consenting and the analysis of conditions. This study focuses solely on the Raz Blanchard site, which is the area between the Cap de la Hague on the Contenin Peninsula in Normandy, France, and the Channel Island of Alderney, as shown in Figure 1.

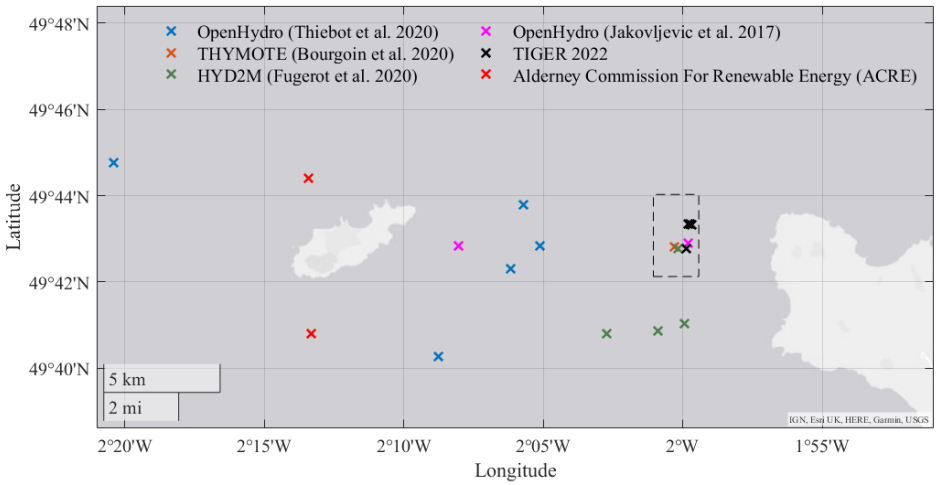

Figure 1. Area map of Raz Blanchard, showing the Channel Island of Alderney on the left and the French coast on the right. Markers have been included to show previous ADCP deployments, with OpenHydro datasets used in [23,24], and the locations of the THYMOTE and HYD2M project deployments given in [14,24], respectively; the dashed box outlines the area of focus in this study, and the domain of this study is shown in detail in Figure 2.

An initial review of the chosen site was conducted to determine the measurement locations that have previously been studied, which are shown in Figure 1. The locations chosen for the previous deployments informed industry, as well as other research projects, [12,14,23–26]. These sets of campaigns have established information about the site in relation to flow properties, although they have drawbacks with the distribution of data post-deployment. Therefore, a new set of ADCP devices were deployed within the TIGER project. The types of devices are listed in Table 1, along with their location and period of deployment. The area of focus is shown as the highlighted area in Figure 1, which is a region of interest to tidal developers, Hydroquest and Normandie Hydrolienne, who are planning to deploy turbines within that area [27].

Table 1. Name, position, and period of deployment for each ADCP deployed in Raz Blanchard as part of the TIGER project.

Device Name	Latitude	Longitude	From	Days
NH1 (Teledyne RDI Workhorse Sentinel 600)	49.72259	−1.9974	15/01/2022	63
NH2 (Teledyne RDI Workhorse Sentinel 600)	49.72225	−1.9946	14/01/2022	61
MU (Nortek Signature 500)	49.72238	−1.9954	15/01/2022	78

Data from the ADCPs allow the vertical profiles of velocity to be determined, resolved from measurements along the beamlines of each device, sidelobe interference near the surface means that 4 metres of data from the surface down are not included in the post-processed data. All three devices have a minimum of four beams in operation, with the Workhorse Sentinel devices having a beam angle of 20° and the Nortek having a beam

angle of 25°. The ADCPs are located within 205 m, with the MU device between the two NH devices, with 145.7 m between the NH1 and MU and 59.3 m between MU and NH2. For each ADCP, the bin size is 1 m, which is the spacing along the vertical, and the sample rate is also consistent at 2 Hz for all current measurements. This sampling rate has been chosen to provide more detail on the change in flow conditions to allow a better prediction of the turbulence at the site. it is worth noting that ADCPs are limited due to the spatial averaging of velocity across multiple beamlines [28], so other devices are being considered for site analysis [29]. In addition to measuring velocities, all three ADCPs are able to determine wave characteristics, such as the significant wave height and peak time period for 30 min samples. The Nortek Signature500 device was also set up with a fifth beam to include acoustic surface tracking and reports on 30 min bursts to provide directional wave spectra. The further analysis of the wave conditions from all three devices and modelled data is shown in Section 4, and the influence of waves on the measured velocities from ADCPs was explored in [30–32].

2.1. Modelling the Resource

Several hydrodynamic models have previously been set up covering the region of Raz Blanchard due to its potential as a tidal site. This work makes use of data from models run by TIGER project partners, the University of Exeter and the University of Caen Normandy, who have models set up which encompass the region around this site. Further details of these models can be found in Table 2. In addition to the measurement campaign, this allows a comparison between measured and modelled conditions at multiple locations within the Raz Blanchard site, as well as the subsequent loading predicted as a function of the model outputs.

Table 2. Resource models used within this study, details of the types of resource modelled, and references with additional detail, a more detailed overview is given in [21].

Model Type	Turbulence Closure	Accounts for Waves	Concurrent with ADCPs	References
Telemac RANS	RANS k-ϵ	No	Yes	[33,34]
Telemac LES	LES	No	No	[16,24]
LBM-LES	LES	No	No	[13,17,35]
Delft3D	No	Yes	Yes	[20,36]

These resource models are able to predict different flow characteristics to varying degrees of fidelity. The extraction points from the models and the measurement locations are shown in Figure 2. The bathymetry data across the site were combined with the measurement locations within the figure. The bathymetry data are provided by the French Hydrographic Office (Service Hydrographique et Océanographique de la Marine, SHOM) with a high resolution of approximately 1 m in the area of interest. Across this site area, it is clear that the bathymetry varies between the extraction locations, with the Telemac-LES ranging from 31.4 m to 53.5 m, and the exact depths of these extraction points were reported in [16]. Across the extraction points within the LBM-LES domain, all nine positions have a similar depth of approximately 35 m. Herein, the Cartesian domains are resolved by 0.25–5 m cell spacing, for the LBM-LES and Telemac LES, respectively, where the LBM-LES spacing becomes coarser towards the free surface. The Telemac-RANS model has been and can be extracted at many different positions and depths across the domain, the focus here is on the locations which correspond to the measurements and other model extraction points. The three measurement locations are approximately 48 m deep according to the bathymetry, and this is consistent with data from the deployed instruments.

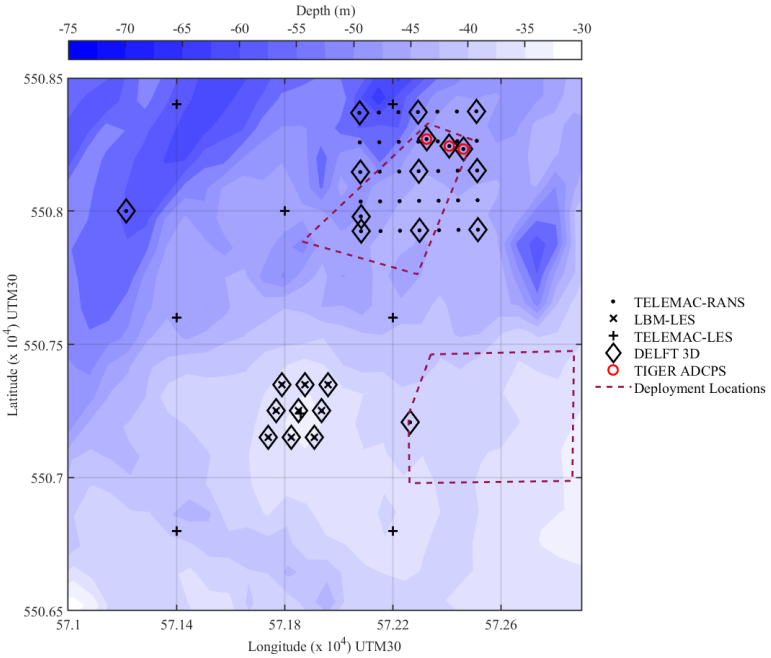

Figure 2. All model and measurement locations across the site at Raz Blanchard. Contours of bathymetry shown by the blue variegation, light to dark corresponding to shallow to deep. Deployment location areas show sites for the development of tidal arrays by developers; Normandie Hydrolienne and Hydroquest [27], domain size shown in figure is 1.9 km by 2 km, grid spacing of 400 m in the horizontal and 500 m in the vertical directions.

The Delft3D model is the only model which includes predicted wave characteristics, with 52 extraction locations. Data have been extracted across the entire site, where the outer model grid has a resolution of 2 km $\times$ 2 km and an inner nested grid around Raz Blanchard has a grid resolution of 100 m $\times$ 100 m. Although data were extracted across the whole area between Alderney and France, the interest in this study is the much smaller highlighted area in Figure 2. From these locations the main aim is to compare the wave characteristics between the three measurement locations and the corresponding model points. These results are presented and discussed in Section 4.

In addition to the data extracted from the wave and current resource model, current and turbulence data are also extracted from the three other models listed in Table 2. The level of fidelity between these three models does vary. With the Telemac-RANS providing data at specific extraction points, in a much larger computational domain. The vertical profiles of velocity and turbulent kinetic energy were extracted over a period of time which corresponds to the ADCP deployments. The next level of fidelity is the Telemac LES model, where grid spacing is 3 m, with 25 vertical sigma layers and a time step of 0.375 s. The data extracted in this study are based upon work conducted during the THYMOTE project which was validated against an ADCP deployment (see Figure 1) [16,24]. This gives some confidence in the model predictions, especially at the model extraction locations nearest the ADCP location. Three periods of time have been focused on, corresponding to a flood and ebb tide in the neap, spring and mean tides. Further details on the original study can be found in [24], and data from all eight locations have previously been shown in [16]. Due to the computational expense of using this model, the same datasets were used in this work to determine the spatial variation in conditions across the site and their impact on loading, specifically the through-life loading. The data provided for 12 h of a mean, neap and spring tide is used to assess the difference in site conditions, specifically the shear and turbulence for different vertical positions across a tidal cycle.

The highest-fidelity model is referred to as the LBM-LES, known as PALABOS, which relies on large eddy simulation (LES) to model the turbulence—based on the lattice Boltz-

mann method (LBM)—which are suitable when modelling with bathymetry; more details on the set-up and details of this model can be found in [13,17,18]. This combination provides a fine spatial resolution with a grid spacing of 0.25 m at the bed, but has a relatively high computational cost, and so each model run tends to focus on a specific set of conditions. In this work, this model was setup to run within the domain, as shown in Figure 2, for both the flood and ebb tides, and for the peak spring tide condition only. The analysis of these conditions will be shown in Section 4, and the influence on the loading when these model conditions are used will also be investigated.

3. Model Set-Up

The overall aim of this work is to improve our understanding of the flow conditions that define unsteady loading experienced on the blades and support-structures of tidal stream turbines. Two different hub heights are used to represent whether a turbine is bed-mounted, referred to as 'near-bed', or floating, referred to as 'near-surface'. The turbine also needs to be defined and used as input to the model, with details given in Section 3.2. From the measured—and predicted—datasets, a full analysis of the conditions is performed as they are required as input to the modelling of the turbine. The specific onset flow characteristics which are investigated from the modelled and measured conditions at the site are given in Section 3.4, with results of the analysis in Section 4. Unsteady flow characteristics for each onset flow interval are employed as input to the turbine load model to determine the time-varying loads. These loads are subsequently used to determine the range of load cycles which occur for each onset flow condition, and hence the fatigue load prediction. Methods used to calculate the time-varying and fatigue loads are provided in this Section. The main processing stages applied to obtain damage equivalent loads from the resource data for a specific location and rotor position are summarised in Figure 3.

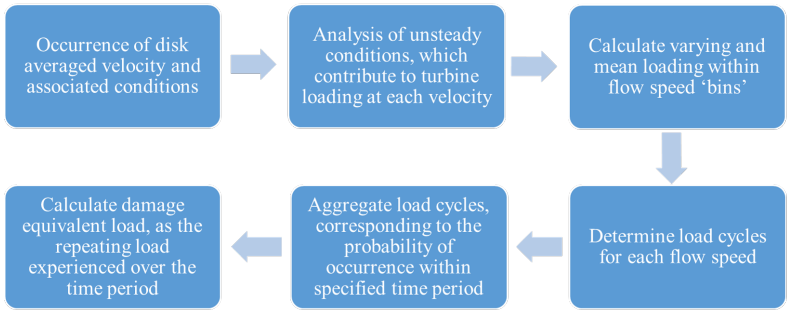

Figure 3. Process used to combine the occurrence and analysis of onset flow conditions with the predicted loading, in order to determine the through-life loading on a turbine component.

3.1. Turbine Fatigue Load Prediction

Similarly to the approach taken in [11,37,38], the fatigue load is quantified using the damage equivalent load (DEL) value. This load is determined using Equation (1), which defines a single magnitude load repeating at a single frequency which would cause the same damage as the time-varying load. This approach facilitates a direct comparison between different unsteady loading cases. The method requires a representative frequency to be used as the value at which the load repeats; in this case, a consistent frequency value is chosen. This corresponds to the rotational speed of the turbine for a single tip-speed-ratio of 5, at the chosen flow speed. Turbine power capping is not considered here, but a cut-in speed of 0.5 m/s is assumed. The load cycles are calculated using the rainflow cycle counting method [39], which was originally defined by Endo et al. (1974) [40], as an algorithm to help determine the cycle size for variable amplitude loading. This counting

method is commonly used for fatigue damage cycle counting and fatigue loads on offshore components have also been calculated using this method [38,41].

$$L_m = \left(\frac{\sum_i n_i L_i^m}{fT} \right)^{1/m} \quad (1)$$

where n_i is the number of cycles at each binned load magnitude, m is the material gradient, f is the repetition frequency, T is the time sample length, L_i is the load bin, and L_m is the DEL for a given material gradient. In this case, m is considered equal to 10, as this represents blades manufactured from glass fibre.

3.2. Turbine Load Prediction in Unsteady Onset Flow

With the method for calculating and comparing the level of fatigue established, knowledge of the turbine geometry and method to calculate the loads is required. As with the turbulent flow field generation, a suitable method is chosen which allows for multiple flow cases to be modelled efficiently. Therefore, the blade element momentum model of [10] is used. The set-up of this model requires turbine geometry, radially varying parameters and the aerodynamic characteristics of the chosen blade profiles. The turbine modelled in this work is the Alstom Energy's DEEP-Gen IV 1 MW tidal turbine, also known as the TGL 1 MW device. Relevant data for this device for this turbine are publicly available [42,43]. This device has a diameter of 18 m and three blades, whilst a single operating point is modelled which corresponds to a tip-speed-ratio of 5.

A basic overview of the method is provided in [10,11]. Initially, a steady-state simulation is run to determine the axial and tangential induction factors, which are used as a single set of values for the unsteady onset flow field calculations. The blades are defined by a series of points 'elements' along the radius. This number can vary depending on the geometry of the blade. With the calculated axial force on each segment of the blade leading to the calculation of flap-wise root bending moment as well as rotor thrust. These results are used to establish the load cycles, (n_i), enabling the fatigue loads to be predicted for the blades. For the input to the BEMT model, other than the turbine characteristics, details on the operating conditions are needed. For unsteady loading, this requires a turbulent onset flow field to be created, and is discussed in the following section.

3.3. Onset Flow Field

There are benefits to using CFD software to create the turbulent flow field, where turbines can be included within the simulation, resulting in a direct interference between the turbine and flow field, useful for looking into wake effects. LES simulations provide the opportunity to generate time-varying turbulent velocity fields but, due to the relatively high computational cost, are predominantly performed for a single operating point, and for a single onset flow condition [2,5,44]. As the interest in this work is to investigate a large number of onset flow conditions, a more computationally efficient approach is instead adopted. Measured turbulent conditions are re-created as input to a loading model using spectral turbulence models, referred to as the Sandia method [45]. In these, power spectral densities (PSD) across a grid of discretised points are combined with a coherence function to create the flow field. The von Kármàn spectrum is commonly used to provide a suitable PSD of the stream-wise velocity [10,22,38,46,47]. This method is defined as a random statistical approach which combines stochastic velocity spectra with auto-spectral density functions to describe real atmospheric turbulence. Adaptation for tidal turbines has not resulted in a new model, but rather the target characteristics are different with application. These models have been created for 'flat' land sites and therefore perhaps at this stage do not completely define sea-bed generated turbulence. A 2D spatial grid of synthetic turbulence is generated which varies in time, propagated using Taylor's frozen turbulence hypothesis [48]. This generation method has been set up using NREL software Turb-Sim. Comparisons in [10,49] have been made using this method to create a flow field with a synthetic eddy method (SEM), developed by [50]. Both methods can be used at low

computational cost to provide a suitable inflow. The onset flow field is set up according to Equation (2), where the unsteady time varying characteristics of the flow can be defined, as mentioned in Section 1.

$$u = \overline{u} + \tilde{u} + \tilde{u_w} + u' \tag{2}$$

where the overall onset flow, u, is created by a mean value, $\overline{u}$, a periodic shear component, $\tilde{u}$, a periodic wave component, $\tilde{u_w}$, and a fluctuating component, u'. The magnitude of the fluctuating component is defined by the turbulence and wave conditions, and the periodic component is defined by the full shear profiles. The characteristics which are used to define the flow field are detailed in the following section.

3.4. Onset Flow Characteristics

Using the data extracted from the measurements and models listed in Section 2, the onset flow is characterised, using the dominant component of velocity in the mean current direction for both the flood and ebb tides. Following the design standards [51], a 10 min average is used to identify the range of onset flow speeds. From all models and measurements the velocities are initially extracted as vertical profiles through the water depth, with the top four metres of the measured profile excluded as previously mentioned. This provides details on the shear profiles, both measured and modelled, and allows for the calculation of a disk-averaged velocity (U_{DA}). To distinguish between the two vertical turbine positions modelled herein, the disk averaged velocity is calculated separately for a turbine with a hub 15 m below the 10 min mean water level as the near-surface turbine, and a hub 15 m above the sea bed for the near-bed turbine. The disk-averaged velocity is calculated using Equation (3), as a power weighted disk average, in accordance with IEC 62600-200 [52].

$$U_{DA} = \left[\frac{1}{A_D} \sum_{i=1}^{n} U_i^3 A_i \right]^{1/3} \tag{3}$$

where A_D is the rotor area, U_i is the velocity at each vertical velocity bin, at depth z, and A_i is the strip wise area of each vertical bin. The vertical bins consider the range from the hub height, z_{hub}, to U_{+R} and to U_{-R}, with the distance between defined by $\pm\Delta U$. The U_{DA} values provide the mean velocity for each onset flow field. It also allows the vertical shear profiles of velocity to be categorised, to investigate any variation in shear with flow speed magnitude. Each 10 min sample from the models and measurements also provides the fluctuations of velocity within the sample. Herein, all velocity fluctuations are considered to be associated with turbulence. In reality, the measured velocity fluctuations contain other environmental effects, such as wave-induced kinematics. Some studies have looked at taking the turbulent kinetic energy from a site, with known wave conditions, to separate out the influence of waves on the turbulence [30,31], or using measured detailed wave conditions to remove the influence [32]. Further discussion on the measured—and predicted—occurrence of wave conditions is given in Section 4.3 but for the purposes of load analysis, the turbulence intensity is defined using Equation (4) only.

$$I = \frac{u'}{\bar{u}} \tag{4}$$

where $\bar{u}$ is the mean velocity and u' is the root-mean-square of the total velocity fluctuations, from waves and turbulence. The ADCP measurements are also used to define the turbulence lengthscales for the creation of the turbulent flow field. For each hub height, a number of samples are extracted, and the lengthscales are calculated at the hub height for each turbine position through the use of an auto-correlation function. A single value of 21 m is used for the site-specific lengthscale, which is used to define the turbulent onset flow field in this work and is the average of the calculated values. This is to determine the impact other flow field features have on the resultant loading.

4. Onset Flow Conditions

Using the parameters defined in Section 3.4, the model and measurement data are used to determine the onset flow conditions. The whole area of interest in Raz Blanchard is covered by the Telemac RANS and Delft3D model. The Telemac RANS spans the measured locations and data points are coincident with the data points of all other model types and so this is considered as the reference case. For the Delft3D model, a comparison of the occurrence and range of wave conditions focuses on wave-conditions at the central ADCP location. The Telemac LES and LBM-LES provide more detailed turbulence information for the conditions, relative to the Telemac RANS, and have been modelled over the same period and locations.

4.1. Occurrence of Conditions

Following the process shown in Figure 3, the occurrence of conditions needs to be established. For each ADCP deployment location, the disk-averaged velocity for the near-bed and near-surface positions has been determined for both the ebb and flood tides. The percentage of occurrence for each binned flow speed is given in Figure 4 where the velocity bin width is 0.2 m/s, consistent with the standards for design [51]. The percentage occurrence is used to highlight that, over the same period as the measurement, there are differences in the conditions. The values are of use to tidal developers when looking for potential energy yields from a site. For the three measurement locations, the predicted occurrences from the model extraction are very similar for both turbine positions during the flood tide. During the ebb tide, for both turbine positions, there is a noticeable difference in occurrence, with the measured conditions experiencing higher occurrence between 0.3 and 1.7 m/s, reduced occurrence at flow speeds greater than 1.7 m/s. This is consistent for both the near-bed and near-surface turbines. This difference for the ebb tide for the Telemac RANS model could be due to the model not being tuned to fit the specific ADCP time-series, it has been calibrated using other ADCP deployments, in different areas in Raz Blanchard. Also within calibration there was no discrimination between flood and ebb tides. The turbulence closure within the RANS relies upon $k - \epsilon$ model, and therefore, is it possible that the predictions of turbulence and hence shape of velocity profiles are poor around abrupt changes in depth such as the shallower depth region in the south west of the site, where the ebb tide flows from south west to northeast. In addition, any imperfections in boundary conditions cause errors to be propagated through the model. However, the RMS error is satisfactory and in the same order of magnitude as found with other models using similar physics. For the near-bed turbine, there is a reduction in occurrence at the higher flow speeds compared to the near-surface turbine, as expected due to the shape of the shear profiles which are present, as shown in Figure 5.

These occurrence statistics can be used to determine through-life loading, allowing the calculation of load cycles to be aggregated into loading over a longer period. Although the modelled occurrence is shown here, the measured occurrence will be used in the lifetime loading calculations.

4.2. Shear Profiles

The occurrence of onset flow speed has been characterised by the power-weighted disk-averaged velocity which accounts for the vertical shear, both measured and modelled. The vertical shear from the measurements and models is incorporated into the simulated onset flow field to determine the loading in the later sections. For all measurement and modelled data, the shear profiles have been determined based upon the 10 min samples and categorised according to the disk-averaged velocity. Therefore, for the near-surface turbine, the sample of shear profiles which correspond to each binned flow speed will be different than those for the near-bed turbine. For one of the measurement locations, at the MU ADCP, the variation of shear profile with the disk-averaged velocity is shown in Figure 5. For both the near-surface and near-bed locations, the ebb tide has no shear cases

where the velocity is greater than approximately 3.3–3.5 m/s which corresponds with the occurrence of calculated U_{DA}.

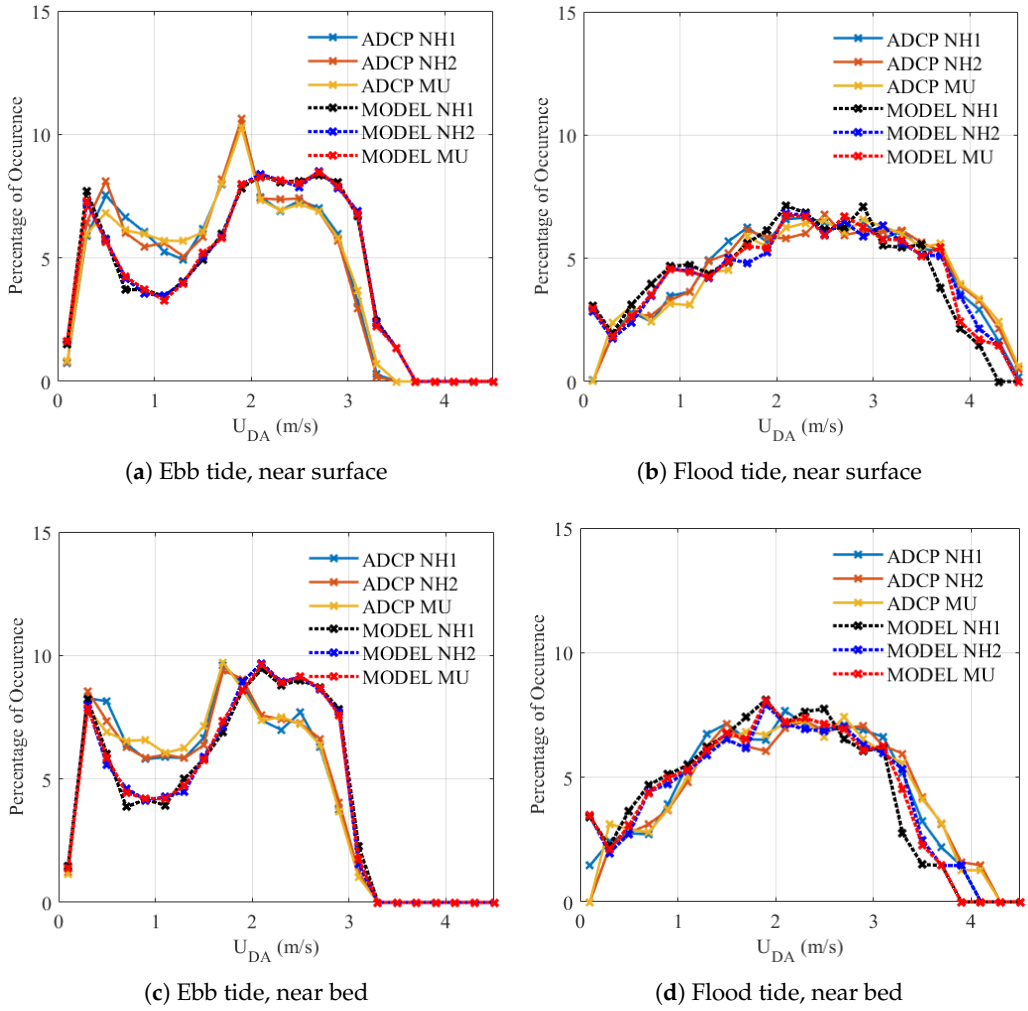

(**a**) Ebb tide, near surface (**b**) Flood tide, near surface

(**c**) Ebb tide, near bed (**d**) Flood tide, near bed

Figure 4. Percentage of occurrence of the disk-averaged flow speeds for the ebb and flood tides for the two vertical turbine positions, using the measurement data from each ADCP (MU, NH1, NH2) and the corresponding model data from Telemac RANS.

A comparison of the range of velocity across the rotor with each disk-averaged velocity bin is shown in Figure 6. This has been calculated for the measurements and from the Telemac RANS data at each ADCP location for the flood and ebb tides, encompassing 95% of the data from each shear profile. For the near-surface turbine, the range of shear across the rotor from the measurement data is significantly greater than that from the modelled data at the lower U_{DA} values. Due to the shear profiles from the measurements having a greater variation across the disk at lower flow speeds, there is more influence from other environmental factors than just the bed roughness. At higher disk-averaged velocities, the range from the model corresponds well with the measurement data, especially in the flood tide for the NH1 and NH2 locations. For the MU location, which lies between the NH1 and NH2 position, the measured range of conditions has less agreement with the model across the higher range of U_{DA}. For the near-bed turbine, the range of velocity across the rotor for both the measurement and model data is higher at higher U_{DA} values. This range is greater than for the near-surface turbine from a range of (approximately 20–40%), as expected from the curvature of the shear profile. Although the range is greater in the lower U_{DA} values, it is not as large as that for the near-surface turbine, highlighting that, in the lower U_{DA} range, other factors such as waves may be impacting the shear profile, and are more visible

in the lower flow speed ranges. These results highlight the variation of shear present at a site.

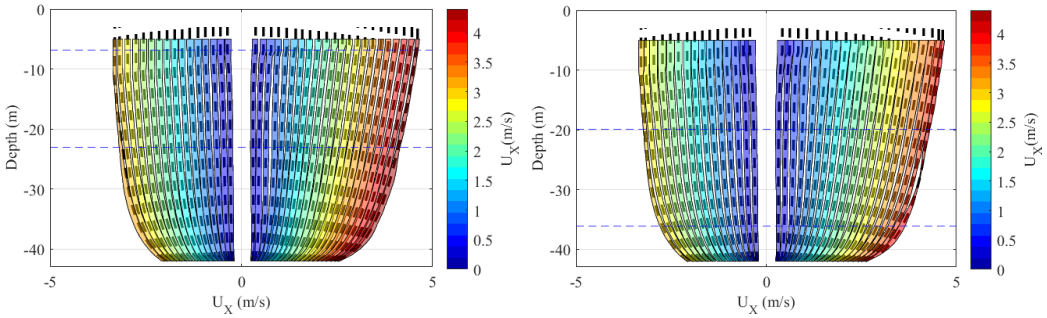

(**a**) Near surface (**b**) Near bed

Figure 5. Variation of shear profile, ±1 standard deviation, for the range of binned disk-averaged velocities, for the near-bed and near-surface turbine location, at the MU ADCP location.

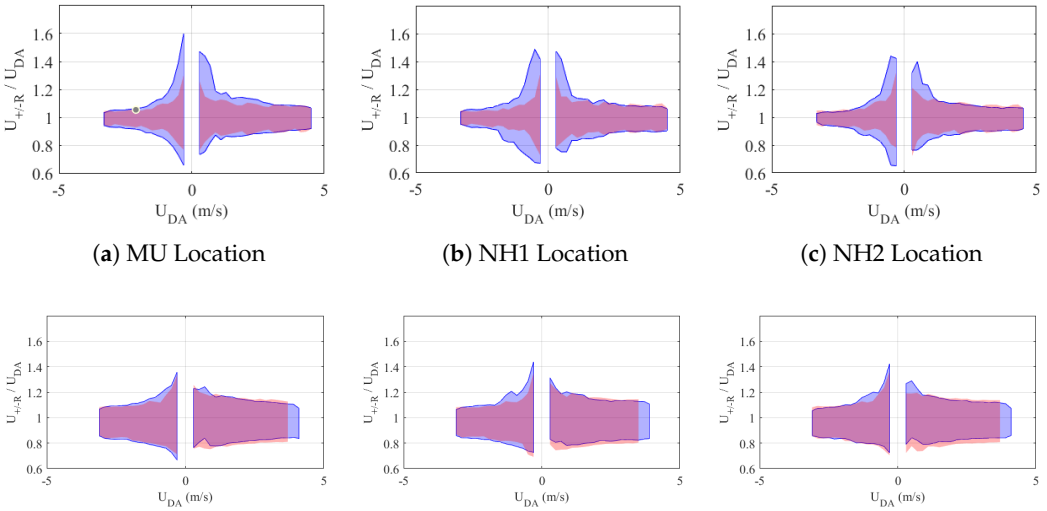

(**a**) MU Location (**b**) NH1 Location (**c**) NH2 Location

(**d**) MU Location (**e**) NH1 Location (**f**) NH2 Location

Figure 6. Normalised across-rotor variations of velocity are compared for each disk-averaged velocity value for (**a**–**c**), the near-surface turbine and (**d**–**f**) for the near-bed turbine, the measurement range is shown by the blue band and the Telemac RANS variation is shown by the red band. For both cases, the range is calculated using 2 standard deviations of the profile values.

Details of the shear profile at one flow speed bin, U_{DA} = 2.2–2.4 m/s, is shown in Figure 7. There are 703 samples within this bin, 301 in the flood tide and 402 in the ebb. The Telemac RANS model was extracted at the same locations as the three ADCP measurements, also shown in Figure 7. For the near-surface turbine positions in Figure 7, the shear in the flood tide is well represented by the model and overlays the measured conditions. In the ebb tide, the measured shear has less curvature than the modelled shear cases, which has a greater gradient across the rotor area. Towards the top of the rotor area, the measured shear profiles become more vertical. For the near-bed turbine, the measured shear profiles have a greater variation in the flow speed bin than for the near-surface turbine, as expected, based on the shear being caused by the features and roughness of the sea bed. The modelled shear profiles also do not follow the same trend as the measured data and have less variation. Across the rotor, the shear is more severe from the modelled data, where the rotor as it rotates will experience a greater variation of velocity, than for the measured data, also shown in Figure 6. The variation in the shear profiles is used to determine the loading on a turbine for each specific condition in Section 5.

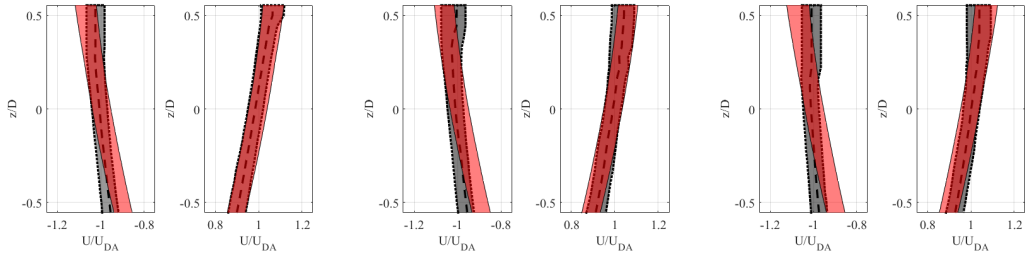

(**a**) MU location (**b**) NH1 location (**c**) NH2 location

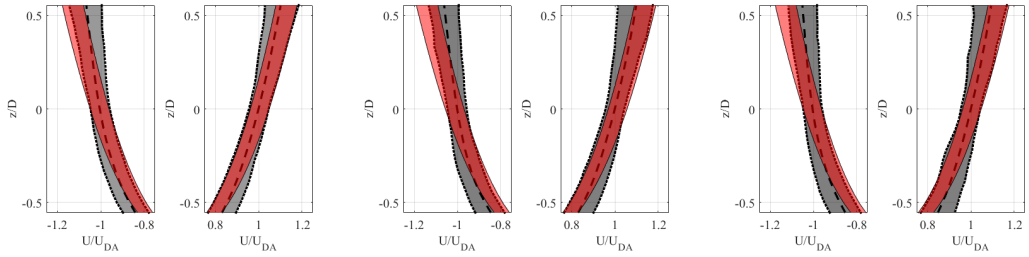

(**d**) MU location (**e**) NH1 location (**f**) NH2 location

Figure 7. Comparison of shear profiles at a single U_{DA} of 2.2–2.4 m/s, over the rotor plane for (**a**–**c**) the near-surface turbine and (**d**–**f**) the near-bed turbine, within a range of two standard deviations, for each ADCP location, as can be seen in Figure 2. Measured mean shown by a dashed black line, and measurement range shown by the grey band, Telemac RANS variation shown by the red band.

For the single design case with a U_{DA} of 2.2–2.4 m/s, a comparison of the variation of velocity across the rotor is made for the Telemac RANS model to the measurements in Figure 8a. The other resource models which model the depth varying current and turbulence, Telemac LES and LBM-LES, have extraction points at different locations to the measurement locations. This is due to the computational expense of running these types of models; the data used here were readily available from the models, with locations shown in Figure 2. The shear profiles from the spring tides were extracted for both the flood and ebb tides for both resource models, and shown in Figure 8b,c. When the comparison of the velocity variation across the rotor between the Telemac RANS and Telemac LES is observed, the Telemac RANS has a greater variation in comparison to the shear determined at the measurement locations, as the data are extracted over a greater range of 1.6 km instead of 0.2 km, with the near-bed turbine in the ebb tide experiencing the greatest shear. The Telemac LES, however, has a reduced shear variation, with the total difference in velocity from the shear less than $0.45\Delta U$, compared to almost ΔU for the Telemac RANS. The shear for the flood and ebb profiles, extracted from the LBM-LES data, are shown in Figure 8c. These profiles are extracted over a much smaller spatial range than the Telemac LES, 170 m $\times$ 200 m. For the near-surface turbine, in the flood tide, there is very little variation in profile across the nine model extraction locations. However, in the ebb tide, the variation is greater across the rotor, with one case having a significant reduction over the bottom half of the rotor. For the near-bed turbine, for both the flood and ebb tides, there is a greater variation of velocity across the rotor area. The shear is expected to be greater closer to the bed based upon the shear being caused by the bed roughness. These shear predictions for a turbine located near the bed from the LBM-LES differ from the predictions from the Telemac LES due to the difference in location. As for both the LBM-LES and Telemac LES, the measured bathymetry is taken into consideration within the model and has a greater impact on the roughness and therefore the shear near the bed. These profiles are not extracted at the three measurement locations and therefore cannot be directly compared. However, impact of these profiles on the spatial variation of the design and through-life

loading at the site is considered further in Section 5. Using the full shear profiles over the rotor, such as Figure 8, but for all U_{DA} bins.

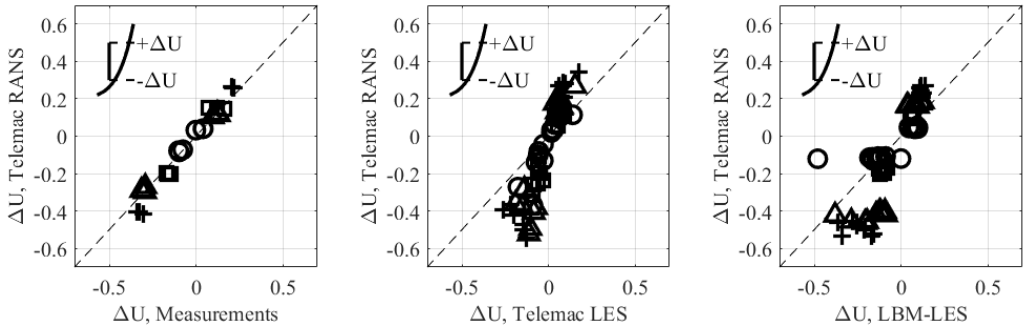

Figure 8. Comparison of ΔU which defines the shear across the rotor for a U_{DA} of 2.2–2.4 m/s, predicted from the three resource models, for the ebb and flood tides and the two vertical turbine positions, where (○) is the near surface in the Ebb tide, (□) is the near surface in the flood tide, (△) is the near bed in the Ebb tide, and (+) is the near bed in the flood tide. (**a**) Measurements versus Telemac RANS (3 locations); (**b**) Telemac LES versus Telemac RANS (8 locations); and (**c**) LBM-LES versus Telemac RANS (9 locations), at the specific extraction locations from Figure 2.

4.3. Waves

The significant wave height and peak time period are compared from the Delft3D model and the ADCP measurements. The occurrence and mean value of wave conditions with disc-averaged velocity for near-surface turbine at the MU ADCP location is shown in Figure 9. All plots within Figure 9 have a range of joint occurrence, where no specific set of conditions occurred more than 1% of the time. There is broad correspondence between the measured and modelled H_S over the time period. Within the flood tide, both the modelled and measured cases are showing a large range of significant wave height, with a maximum of approximately 5 m for the modelled case. There is a similar peak wave period for the ebb tide but a differing trend in the flood tide between the modelled and measured conditions.

An additional comparison has been made to a full year of modelled wave conditions and to a period corresponding with the measurements (January–March), which is shown in Figure 9c,d. Across the year, the average occurrence of the significant wave height with each disk-averaged velocity is lower than that for the smaller sample period. For the peak time period, the use of a full year of data has also led to a reduction in mean value at each U_{DA} value, as expected since the measurement period occurred during winter. Understanding the occurrence of these conditions at a site from the model and measurements allows for the determination of the impact that waves are having on the flow characteristics. It is clear from the full-year comparison that a reasonable prediction of occurrence at a site can be found. Although there is no consideration given to the wave heading, these data are also available from the measurements and the model.

Based on the measured conditions, waves with $H_S > 0.5$ m and with period greater than 3 s may be expected to impact kinematics to mid-depth and these conditions occur with all disc-averaged velocities. The waves occurring at this site may therefore be expected to have some impact on turbulence intensity, but at this stage, no attempt has been made to separate wave-induced kinematics from turbulence. An initial study of the treatment of wave kinematics on both the value of turbulence intensity obtained from measurements, and the modelled fatigue loads is given in Mullings et al. [32].

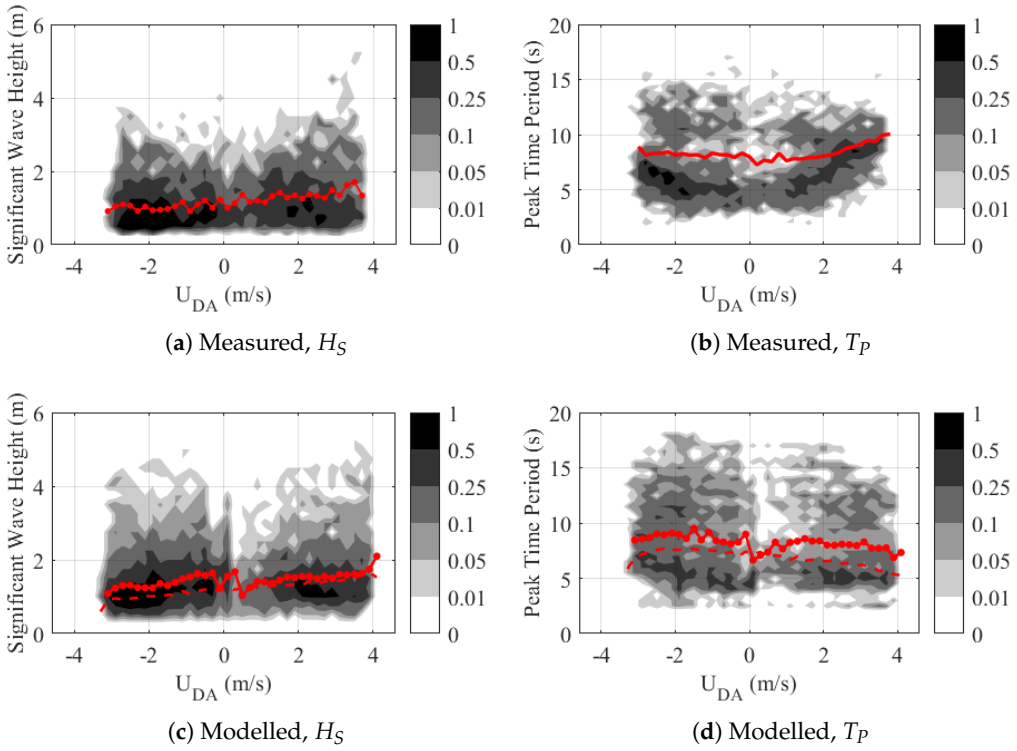

(**a**) Measured, H_S (**b**) Measured, T_P

(**c**) Modelled, H_S (**d**) Modelled, T_P

Figure 9. Joint probability of the occurrence of the significant wave height (H_S) with the disk averaged velocity (U_{DA}) for the measurement data at one ADCP location, MU see Figure 2, and the peak wave time period (T_P) with the disk-averaged velocity, with the mean of each condition at the near-surface U_{DA} values for the measurement period, as shown in red (solid line) and the mean over an annual interval for the modelled case in red (dashed line).

4.4. Turbulence

Turbulence has been investigated using the ADCP measurements and three of the hydrodynamic models, the two Telemac models and the LBM-LES, to assess the variation of measured and predicted turbulence intensity. The range of intensity for each binned onset flow speed is used within the loading model for the turbine at a single design case. The mean intensity values from the measurements and each model are also used to determine the through-life loads across the range of disk averaged velocities.

For the measured cases, the intensity is calculated using Equation (4), and for each 10 min averaged case, the intensity is calculated across the depth. This includes the influence of the waves as well as turbulence, this is referred to as turbulence intensity throughout. The intensity values reported here have been calculated as a disk average following the same method applied to the onset flow velocity using Equation (3). For each measurement location and for the two turbine hub heights, the variation in turbulence intensity is shown in Figure 10. For the turbine located near the surface, the measured disk average turbulence intensity is greater in the lower disk averaged flow velocity range (<1.5 m/s), than a turbine located near the bed. However, at higher disk-averaged velocities (>1.5 m/s) the calculated intensities are lower for near the surface than near the bed. One reason for this could be the influence of the bed generated turbulence on the flow field for the near-bed turbine. However, at the near-surface turbine, the variation in the turbulence intensity is also greater at the lower flow speeds. The influence of the flood and ebb tides on the measured turbulence intensity has little impact near the surface location, but at the near-bed position, there is a definite difference with the flood tide providing higher intensity values. The influence of the range of turbulence intensity values from the measured data on the loading experienced by a turbine is explored further for a single U_{DA} 'bin'.

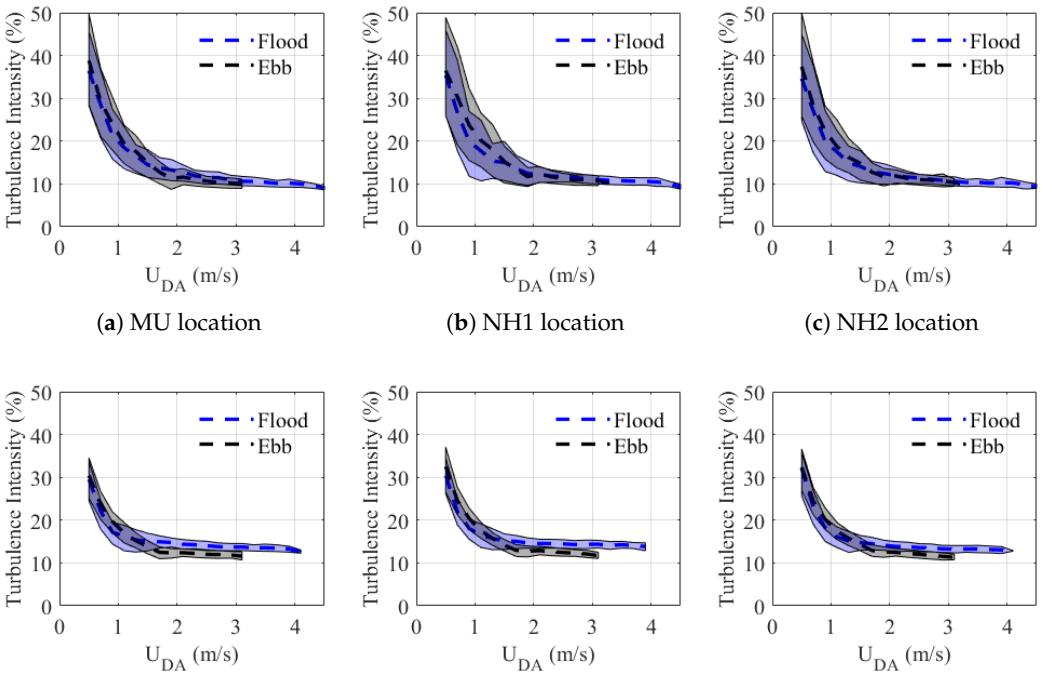

Figure 10. Mean and variation to within one standard deviation of the intensity with disk-averaged velocity for the ebb and flood tides for each ADCP location, given in Figure 2, near the surface (**a**–**c**) and near the bed (**d**–**f**).

The three hydrodynamic resource models also provide turbulence intensity values. The Telemac RANS model provides the turbulent kinetic energy at each ADCP location as well as a further 55 points. The turbulent kinetic energy is determined through the $k - \epsilon$ turbulence closure model. Comparing the mean disk-averaged turbulence intensity variation with the disk-averaged flow speed, it is found that the calculated values of turbulence intensity from the model are lower than the measured cases for both vertical turbine positions and the flood and ebb tides. A comparison of the mean intensities calculated at the three locations for the measurements at one U_{DA} value (2.2–2.4 m/s) against the Telemac RANS model is given in Figure 11. It is clear that, at this U_{DA} value, the Telemac RANS under-predicts turbulence, which would be expected from a model which does not resolve the larger bed-generated turbulent structures within the flow field. For this case, across the measured locations for both vertical turbine positions, there is less than 1% difference in the calculated mean turbulence intensity, within the measured cases and for the modelled cases.

When looking at the variation between measurement locations, there is a slight trend with the largest mean intensities found at the NH1 location decreasing as the measurement devices are placed further east, but this difference is as mentioned before within the 1% across the turbulence intensity values. The mean intensities for the modelled cases are smaller than the measured cases, with a reduction of up to 63%. The measured conditions are driven by a wider range of processes, such as waves and bed-generated turbulence which can vary with irregular bathymetry. With the near-bed turbine experience giving higher mean intensities, it is thought that the bed generated turbulence has more influence than other environmental factors.

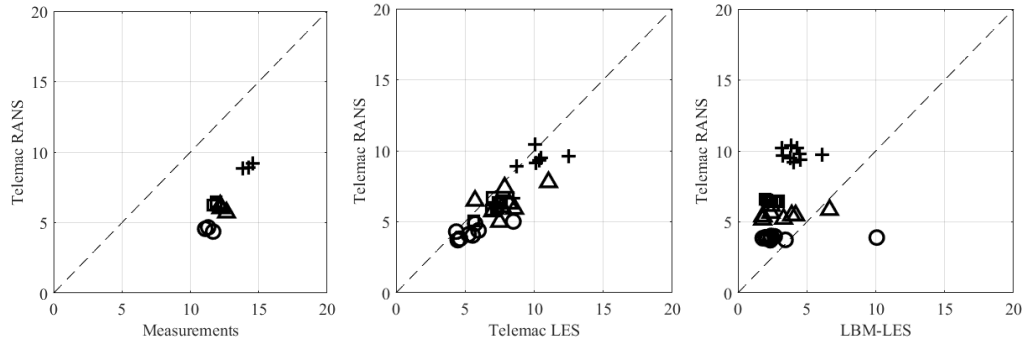

Figure 11. Comparison of the mean disk-averaged turbulence intensity for a U_{DA} of 2.2–2.4 m/s, predicted from the three resource models, for the ebb and flood tides and the two vertical turbine positions, where (○) is the near surface in the Ebb tide, (□) is the near surface in the flood tide, (△) is the near bed in the Ebb tide, and (+) is the near bed in the flood tide. (**a**) Measurements versus Telemac RANS (3 locations); (**b**) Telemac LES versus Telemac RANS (8 locations); and (**c**) LBM-LES versus Telemac RANS (9 locations), at the specific extraction locations from Figure 2.

For a better turbulence prediction, the Telemac LES model is used, and this method resolves the larger turbulent eddies within the model capturing the variation in flow over a wider range of frequencies. The data are extracted at eight locations across the site, with one of these locations corresponding to an ADCP deployment as part of the THYMOTE project [16]. Corresponding data were also extracted at the same locations from the Telemac RANS model. This model is less computationally expensive to run and therefore it is helpful to compare the flow conditions to understand whether it is necessary to include the large eddy simulations. A comparison of the mean disk-averaged turbulence intensities is shown in Figure 11 for both vertical turbine positions, as well as the flood and ebb tides at the same U_{DA} value as the previous measurement comparison. The overall trend highlights the under-prediction from the Telemac RANS model when compared to Telemac LES. The large range of predicted intensities for the single U_{DA} case, from 3.7% to 11% for the Telemac RANS model and from 4.3% to 12.5% for the Telemac LES.

The data from the LBM-LES represent the highest onset flow across a very specific set of locations in Raz Blanchard, as shown in Figure 2. These simulations are used to define the velocity profile and turbulence of a fully developed profile. The range of disk-averaged velocity for these cases is 3.7–4.5 m/s; at these values, based on the previously observed relationship from the measurement data, the turbulence intensity is expected to be constant and represent the lower U_{DA} value. The predictions of the mean disk-averaged turbulence intensity from this model are compared to the Telemac RANS predictions at the same locations for the maximum flow speed predicted by the Telemac RANS and for the single U_{DA} of interest for the design case comparison. It was found that, for the disk-averaged velocities predicted between the U_{DA} of 2.2–2.4 m/s and the maximum value, there is no change in the predicted disk averaged turbulence intensities from the Telemac RANS model. The comparison of the two models at the nine locations, for the flood and ebb tides and the two vertical positions, is shown in Figure 11. With the largest difference in the prediction intensity found for the near-surface turbine in the ebb tide at the central easterly location, the LBM-LES has an intensity of 10.1% and the Telemac RANS predicts 3.9%. As with the earlier model comparison between the Telemac RANS and Telemac LES, the near-bed flood tide conditions provided the highest predictions of turbulence intensity for these extraction locations, in the range of 9.2–10.4%, but only 3.2–6.1% for the LBM-LES. Other than at one location, the near-bed turbine in the flood tide has a greater predicted intensity than the all other conditions and has greater intensities than all of the near-surface predictions in the flood tide.

4.5. Spatial Variation of Turbulence

The models also reveal more information about the spatial variation across the site due to the greater distances between extraction locations. The variation in these intensities is shown in Figure 12 for the Telemac LES and the Telemac RANS at the same extraction locations. For the near-bed turbine in the ebb tide, the intensities range between 5% and 11% for the LES model and from 5% to 8% for the RANS model. The near-surface turbine in the ebb tide has a range of 3.7% to 5.2% for the RANS model and 4.3% to 8.5% for the LES model. As with the ebb tide, for the flood tide, the near-bed turbine experiences a greater mean disk-averaged turbulence intensity than the near-surface turbine for which the range is 5–6.3% for the RANS model and 5.6–7.5% for LES model. For the near-bed turbine, the RANS model predicts a range from 6.6% to 10.4%, and for the LES model, the intensity varies from 8.5% to 12.5%. The areas of high-to-low intensity vary depending on the tidal direction and vertical position. There are higher intensities in the south/southwest of the domain on the ebb tide for both modelling methods, and the reverse for the flood tide. The area of the ridge towards the South of the domain may contribute to the lower intensities observed compared to the rest of the domain for both tidal directions.

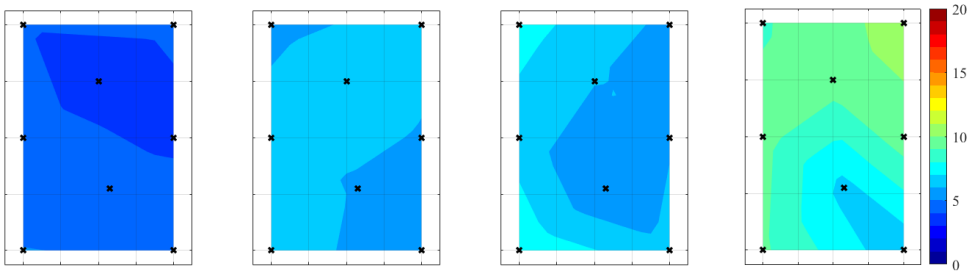

(**a**) Near surface, ebb (**b**) Near surface, flood (**c**) Near bed, ebb (**d**) Near bed, ebb

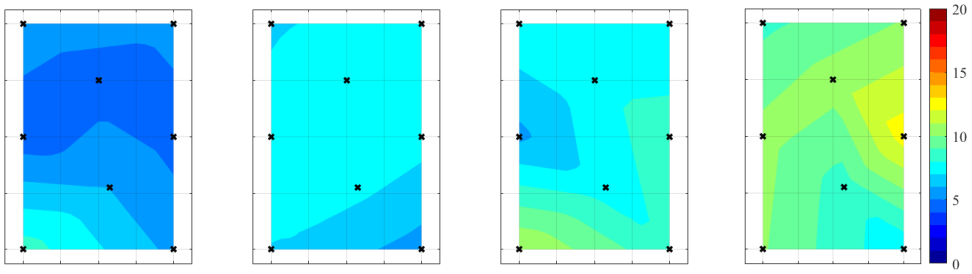

(**e**) Near surface, ebb (**f**) Near surface, flood (**g**) Near bed, ebb (**h**) Near bed, flood

Figure 12. Spatial variation of mean turbulence intensity at the single U_{DA} value (2.2–2.4 m/s), scale shown in (**d**,**h**) and is consistent across the figure, for (**a**–**d**) Telemac RANS and (**e**–**h**) Telemac LES, in the flood and ebb tides and for the two vertical turbine positions for the eight locations given in Figure 2 for the Telemac LES.

The spatial variation of the turbulence intensity extracted from the LBM-LES profiles is shown in Figure 13, again compared to the Telemac RANS model at the same extraction locations. As the LBM-LES includes the bathymetry and resolves the larger turbulent eddies, the intensities from this model should include a good estimation of the bed-generated turbulence which is observed in these values. A recent study by Mercier et al. [53] using this method has shown that the turbulence intensity does not necessarily correlate with the bathymetry, turbulent structures can be initiated upstream, so whilst there is some relationship, turbulence intensity does not directly correlate with the bathymetric depth. During the ebb tide, one location has a much greater intensity for the near-surface turbine; however, the remaining values are very similar, within 1.5%. This highlights that, in the

ebb direction, the bed-generated turbulence does not have a sustained impact across the locations, with the near-bed predictions not being consistently higher than the near-surface predictions. Due to the smaller spatial separation of the model extraction locations, there is very little difference in turbulence intensity across the locations. The points are centred around a shallower ridge in the bathymetry, as observed in Figure 2. For the Telemac RANS, the difference observed between the ebb and flood intensity magnitudes for each position highlights that the intensity may be impacted by the transition from the deeper northwesterly direction as the flow moves south, as previously mentioned in the set-up of the model.

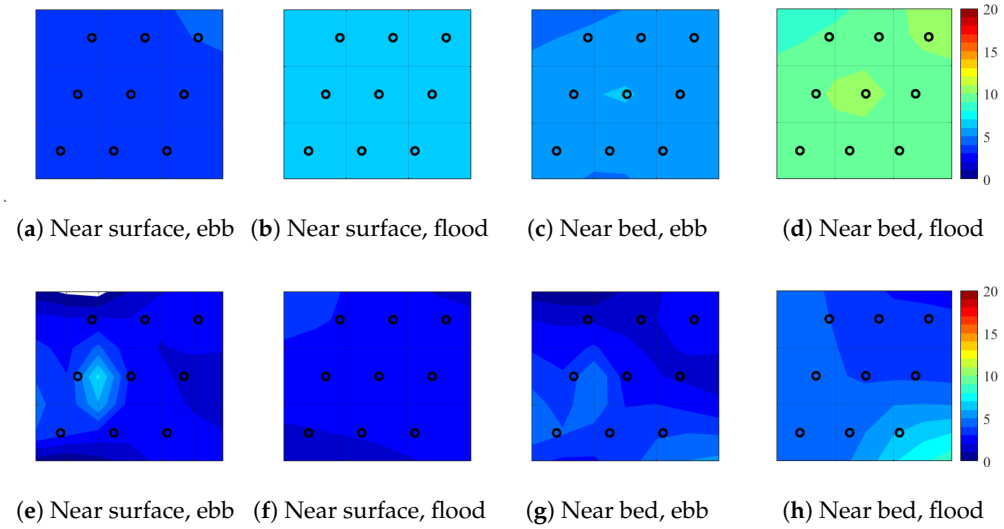

(**a**) Near surface, ebb (**b**) Near surface, flood (**c**) Near bed, ebb (**d**) Near bed, flood

(**e**) Near surface, ebb (**f**) Near surface, flood (**g**) Near bed, ebb (**h**) Near bed, flood

Figure 13. Spatial variation of mean turbulence intensity at the single U_{DA} value (2.2–2.4 m/s), scale shown in (**d**,**h**) and is consistent across the figure, for (**a**–**d**) Telemac RANS and (**e**–**h**) LBM-LES, in the flood and ebb tides and for the two vertical turbine positions for the nine locations given in Figure 2 for the LBM-LES.

5. Loading on a Device

The unsteady loading that a tidal stream turbine will experience is investigated using both the measurement and model data. A single operating point is considered using a disk-averaged velocity of 2.2–2.4 m/s to highlight the potential variation in loads that a device can experience when operating under unsteady onset flow conditions. Using the device scale model set out in Section 3, the modelled and measured conditions are combined with a von Kármàn turbulence spectra model. This is extended to consider spatially varying loads at the single design case and through-life loading over a 5-year period. For consistency all loads reported are normalised by the peak loading experienced for the single design case.

5.1. Influence of Site Location

The blade and rotor loading was calculated in this section based on the ADCP measurements from three locations on the site. The variation of the normalised average damage equivalent loads, calculated from the root bending moments on the three blades, is shown in Figure 14. Across the measurement locations for the near-bed turbine, there is a 2.2% variation in the loads for the ebb tide and a 4% variation for the flood tide, when varying turbulence intensity is included in the flow fields. The mean turbulence intensity was also applied as a constant with the varying shear profiles, the difference in the loads between the varying and mean turbulence intensities is also shown in Figure 14. For the near-bed turbine, the mean turbulence intensity resulted in a 1.2–1% reduction in loads across all three locations and with the same decrease determined for the flood tide. The influence of the mean turbulence intensity on the loads over the varying intensity shows that, for a

near-bed turbine where the variation in turbulence intensity for a design case is less than 7% with a standard deviation of 1.7%, the mean flow predicts loading to within 1.2%.

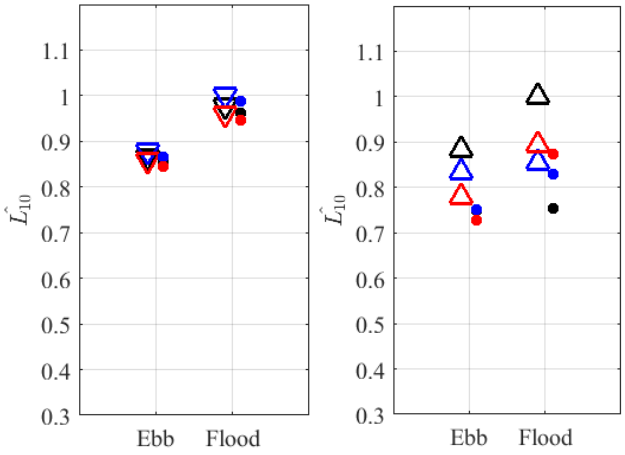

(**a**) Near-bed turbine (**b**) Near-surface turbine

Figure 14. Normalised damage equivalent loads ($\hat{L}_{10}$) from the root bending moment for (**a**) a near-bed turbine and (**b**) a near-surface turbine using varying turbulence (triangles) and a mean turbulence intensity (circles), for the MU ADCP (black), NH1 (blue) and NH2 (red).

For the near-surface turbine, there is a greater difference in the loads with location than for the near-bed turbine. In the ebb tides with varying turbulence, the loads applied at the MU ADCP location are 10.4% greater than at the NH2 ADCP location, separated by 59.7 m, and 5% greater than at the NH1 location, separated by 145.7 m. In the flood tide, the varying turbulence in the loads applied at the MU ADCP location was also greater than those at the other two locations, by 10% to the NH2 location, consistent with the load variation in the ebb tide, and 14.5% greater than the loads experienced at NH1, which is a greater difference than the ebb tide. When the loads using the mean turbulence intensity are considered, for the ebb tide, there is a 15% decrease at the MU ADCP location, a 10% at the NH1 ADCP location, and 7% at the NH2 ADCP location. The mean intensity for all three locations is very similar, with less than 1% difference in the intensity values, which corresponds to the loads being within 3% for the ebb tide. With the varying intensity, the MU ADCP has the greatest variation in intensity at 16.4%, which reduces to 14.7% for NH1 and 11.1% for NH2. The influence of the turbulence intensity values is shown in the loading predictions, with the greatest loads in the flood tide corresponding to the intensity varying by up to 23%.

It is also worth noting the difference in loads between the ebb and flood tides. The turbine experiences a higher loading on the flood tide for all three locations by up to 13% across both vertical positions. For this single design condition and operating point, the same turbine can experience a 27% difference in the calculated load, depending on vertical position, site location within the 205 m separation of the measurement points, and choice of measurement values used. The influence of the modelled data on the load predictions is shown in the following section, initially based upon the Telemac RANS model, before incorporating higher fidelity turbulence model predictions.

5.2. Influence of Modelled Conditions

The initial model used in these load predictions is the Telemac RANS model using extraction points corresponding to the ADCP locations. The extracted model values were used in the same way as the measurement values in the previous section. For a single design case, one onset flow speed bin and operating point, the damage-equivalent loads calculated from the root-bending moments on the blades are shown in Figure 15.

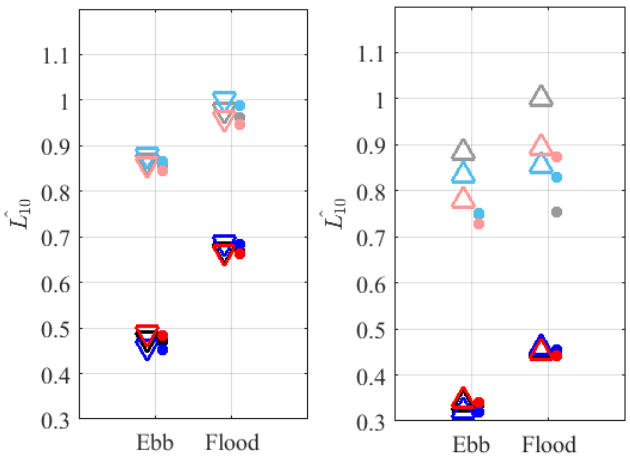

(**a**) Near-bed turbine (**b**) Near-surface turbine

Figure 15. Normalised damage equivalent loads for (**a**) a near-bed turbine and (**b**) a near-surface turbine, using varying turbulence (triangles) and a mean turbulence intensity (circles), determined from modelled data using the Telemac RANS modelling at the ADCP locations, MU location (black), NH1 location (blue) and NH2 location (red), with previous measurement results in greyscale.

For the near-bed turbine in the ebb tide, there is a 3% variation in the loading using the varying turbulence intensity, which is consistent with the range of loads calculated using the mean turbulence intensity; however, the loads are 0.5% smaller. In the flood tide, there is a 2.3% difference across the locations using the varying turbulence replicated using the mean turbulence intensity in the loading simulations. There is a less than 0.3% difference in loads calculated using the mean value of intensity instead of the varying turbulence intensity values. The impact on the loading from the inclusion of different turbulence values is a direct consequence of the lack of variation in the modelled turbulence values with the ebb tide providing a 1.26% variation in predicted turbulence intensity and 0.92% variation for the flood tide. The ebb tide conditions produce loads which are 20% lower than the modelled flood tide for this single operating condition. The turbulence intensity for the near-bed turbine does decrease by between 2.6 and 3.5% across the locations, which does contribute to the reduction in predicted loads.

For the near-surface turbine, the calculated damage equivalent loads from the blade root bending moments are less than the loads predicted for the near-bed turbine. For the ebb tide, the loads vary by 2.2% across the locations with the varying turbulence and have the same variance as when the mean turbulence is used—although these loads are around 0.4% lower. In the flood tide, the loads vary by 1% between the three locations for the varying turbulence predictions and there is a slightly greater variation of 1.3% when the mean turbulence intensity is used in the calculations. The use of mean turbulence intensity also reduces the predicted loads by 0.8%, which is due to the increase in variation of the intensity values; for the ebb tide, this was 1.3%, and for the flood, it increases to 1.8%. As for the near-bed turbine, the near-surface turbine also experiences greater DEL in the flood tide, but the difference is smaller at 12%.

The loads calculated from the model values are compared to the loads calculated from the measured conditions in Figure 14. For the near-bed turbine, in the ebb tide, these are predicted to be around 40% lower when using the modelled conditions and 32% lower in the flood tide. For the near-surface turbine in the ebb tide, the reduction in loads varies from 43% at the NH2 ADCP location to 55% at the MU ADCP location when the varying turbulence intensity is considered. In the flood tide, there is a similar decrease in loads from 41% at the NH1 ADCP location to 56% at the MU ADCP location. The only difference between the loading calculations for each case are the onset shear and turbulence conditions. One way of determining the impact that the turbulence and shear have as independent

conditions is to modify the set-up of one of the cases. To assess this, the modelled shear conditions are used, but the turbulence from the measured conditions was applied, both as a mean value and as a range of intensity values. The influence of the measured turbulence intensity combined with the modelled shear is shown in Figure 16.

Inclusion of the measured turbulence values can be seen to have increased the predicted loads across both vertical positions and across all three ADCP locations. The increase in loads for the near-bed turbine in both the ebb and flood tides means that they are within 1% of the original measured loads, an increase in 40% on the original modelled load values. For the near-surface turbine, the measured turbulence values also increased the load prediction—however, not to the same level as the original measured values. Loads during flood tide remain 10% lower for the MU ADCP location and 7% lower for the NH1 and NH2 ADCP locations, respectively. This is a 45% increase in the load for the MU ADCP location relative to the previous modelled load values due to the change in turbulence intensity.

If measured turbulence values are not available to use as input to a loading model, higher fidelity turbulence models could be used to provide a closer estimate of turbulence to the real site conditions. Two of these higher fidelity models were introduced in Section 2.1, although they don't show a better agreement of turbulence intensity, the turbulence variation and influence on the chosen onset flow speed point of interest (U_{DA} = 2.2–2.4 m/s) is investigated.

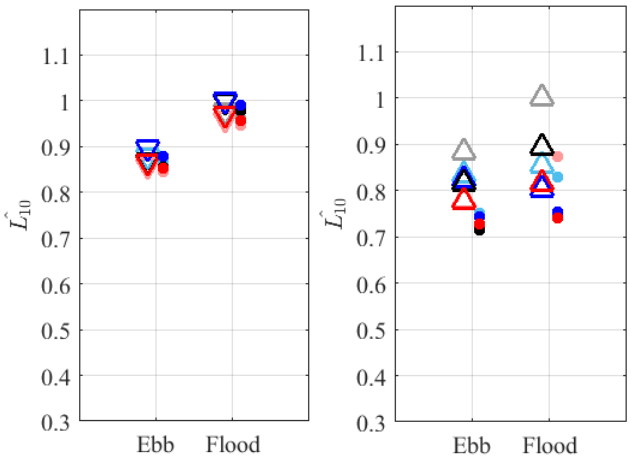

(**a**) Near-bed turbine (**b**) Near-surface turbine

Figure 16. Normalised damage equivalent loads for the two vertical turbine positions using varying turbulence (triangles) and a mean turbulence intensity (circles) determined using the modelled shear data using the Telemac RANS modelling at the ADCP locations and combined with the measured turbulence from the ADCPs modelling at the ADCP locations, which is shown by MU location (black), NH1 location (blue) and NH2 location (red), with previous measurement results in greyscale.

5.3. Influence of High-Fidelity Turbulent Conditions

The loading on the device considered so far has focused on the three ADCP deployment locations. Spatial variation of loading across wider regions of the site is investigated using the resource models introduced in Section 2. Direct comparison between the Telemac RANS and the measurement locations is facilitated by the ease and speed of modelling using the RANS-based Telemac model. Two higher fidelity models have also been used to model this site to look to characterise the turbulence and the spatial variation of conditions [12,13,16]. Firstly, the Telemac LES model conditions were used to determine the spatial variation under conditions for the same, single, design condition, U_{DA} of 2.2–2.4 m/s, and this is compared to the Telemac RANS across the same extraction locations, with the applied conditions shown in Section 4. This comparison is shown in Figure 17.

Across all four conditions, the Telemac LES consistently predicts a higher DEL, which means that the use of the Telemac RANS could result in an under-prediction of the load

cycles which contribute to turbine fatigue. These findings correspond to the measurement comparison in which the Telemac RANS calculations were considerably lower than using the measurement conditions. For all Telemac RANS cases, the ebb tide results in lower DELs compared to the flood at the same vertical position. When comparing the previous Telemac RANS DELs to these predictions, there is a greater variation. The spatial variation across the site for the Telemac RANS is clearly shown for each case in Figure 17. For the ebb tide, there is a 9% variation in predicted DEL for the near-surface turbine and 20% variation for the near-bed turbine. In the flood tide, there is an 11% variation across the site for the near-surface turbine and 27% for the near-bed turbine position. The lowest location across the site is not in the same position for each condition. For the Telemac LES, the DEL vary across the site for the ebb tide by 30% for the near-surface position and 34% for the near-bed position. For the flood tide, the variations across the site are similar for the near-bed position with a 34% difference, but the difference reduces for the near-surface position to 15%. Compared to the variation across the ADCP deployment locations there is a considerable variation in loads with location. When looking at the spatial variation, it is important to consider the variation of loads that will occur over a lifetime, which will be explored in the next section.

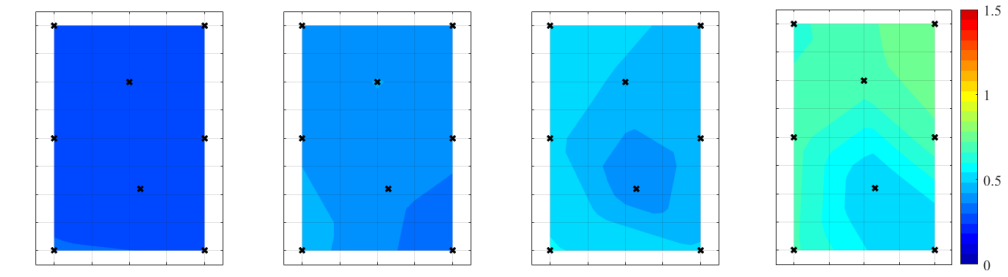

(**a**) Near surface, ebb (**b**) Near surface, flood (**c**) Near bed, ebb (**d**) Near bed, flood

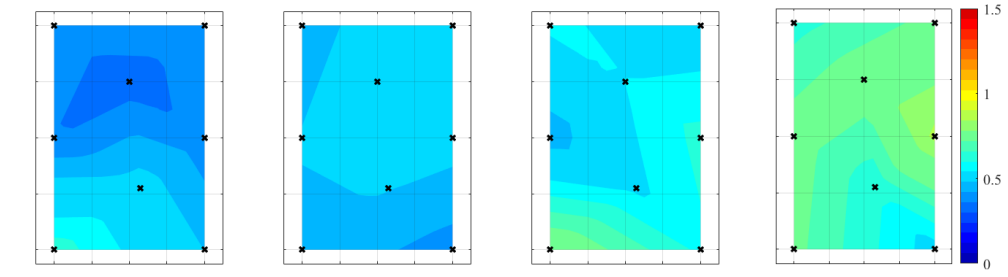

(**e**) Near surface, ebb (**f**) Near surface, flood (**g**) Near bed, ebb (**h**) Near bed, flood

Figure 17. Variation in the normalised damage equivalent loads from the root bending moments when the disk-averaged velocity is 2.2–2.4 m/s, scale shown in (**d**,**h**) and is consistent across the figure, for the eight different site locations, and for the ebb and flood tides at the two turbine positions, using the input flow conditions from the Telemac RANS model (**a**–**d**) and the Telemac LES model (**e**–**h**), for the eight locations given in Figure 2 for the Telemac LES.

The final model used to define the spatial variation in conditions is the LBM-LES. The maximum flow speeds modelled by this method are in the range of approximately 3.7–4.5 m/s. In order to compare the loading in an operating range of 2.2–2.4 m/s, the shear and turbulence intensity values determined for the peak spring tide were used. The loading results are shown in Figure 18, which provides the normalised damage equivalent load values for the blade root bending moment across the nine model extraction locations for the two turbine positions in both the flood and ebb tides. The loading experienced using the conditions from the LBM-LES model were normalised using the same value as

the previous results within this section. The general trend of the loading corresponds to the variation in turbulence intensity with the location, tide, and position given in Figure 13.

The loads predicted from the LBM-LES across the nine locations are compared to the loads predicted from the Telemac RANS at the same locations, as shown in Figure 18. For the Telemac RANS model, there is very little spatial variation across the nine positions, partly due to the proximity of the locations. There is less than 1% variation for the near-surface turbines across all locations and for the near-bed turbines in the ebb tide. For the near-bed turbine in the flood tide, there is a greater variation across the locations of 4%. In comparison with the LBM-LES loading, the Telemac RANS predicts a higher DEL, as expected due to the higher turbulence intensities observed. Across the domain, the LBM-LES has very little variation in DEL, showing a consistent trend in the turbulence intensity findings. At the measured locations, the DELs are greatest for the near-bed turbine in the flood tide, which is also the case for the additional extraction positions across the site.

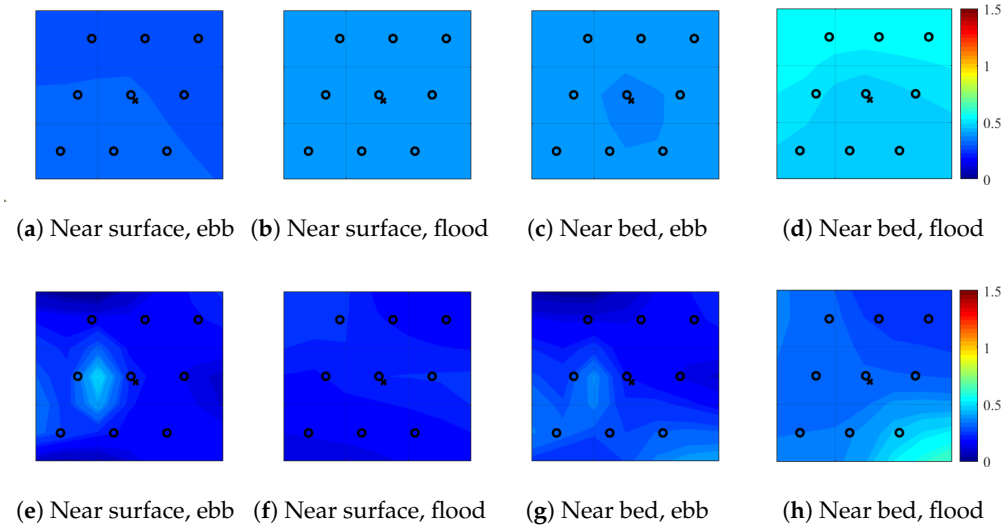

(**a**) Near surface, ebb (**b**) Near surface, flood (**c**) Near bed, ebb (**d**) Near bed, flood

(**e**) Near surface, ebb (**f**) Near surface, flood (**g**) Near bed, ebb (**h**) Near bed, flood

Figure 18. The spatial variation in damage equivalent loads, calculated for the single disk-averaged velocity case (2.2–2.4 m/s), scale shown in (**d**,**h**) and is consistent across the figure, for the nine different site locations, for the ebb and flood tides at the two turbine positions, for (**a**–**d**) the Telemac RANS model and (**e**–**h**) the LBM-LES model, for the nine locations given in Figure 2 for the LBM-LES.

5.4. Through-Life Loading Across Sites

The through-life loading calculated here is based upon the methodology outlined in Figure 3 using the mean modelled and measured conditions across all disk-averaged velocities. The load cycles from these conditions are combined with the probability of occurrences established from the occurrence of all the measured disk-averaged velocities. A five-year period is chosen to represent a realistic blade operating life before any maintenance is due. The modelled probability of occurrence could also be used. During this period, the ebb and flood tides are considered to occur over an even split of a year. Initially, the Telemac LES model extraction points are used to examine the spatial variation. These model extraction points are compared for both the Telemac LES and Telemac RANS, as shown in Figure 19. The DELs which were calculated consider the load cycle variation for the combined flood and ebb tides for the near-surface and near-bed turbines. For both models, the spatial variation differs between the two turbine locations, with areas of higher loading in different locations. For the Telemac RANS model, the greatest DELs were found in the southwest of the site for the near-surface turbine, but in the northeast for the near-bed turbine. When the variation in DEL was compared to the bathymetry, the deepest parts of the site correspond to the larger loads for the near-bed turbine. This is also consistent with the DELs calculated from the Telemac LES model, as shown in Figure 19c,d. At one location in the site, for the near-bed turbine, there is a 16% difference between the

two models, with Telemac RANS producing lower calculated DELs. For the near-surface turbine position, the models produce DELs which vary by 27%, with the Telemac LES producing loads which are greater across every location at the site, when compared to the Telemac RANS DELs. Spatially, the DELs are found to vary by 22% near the surface for the Telemac RANS and 23% for the Telemac LES, so although the magnitude is greater for the LES model, there is a very similar variation across the site. For the near-bed turbine, the spatial variation calculated in DELs is 31% which increases for the Telemac LES model to 39%, with a magnitude which is closer across the site.

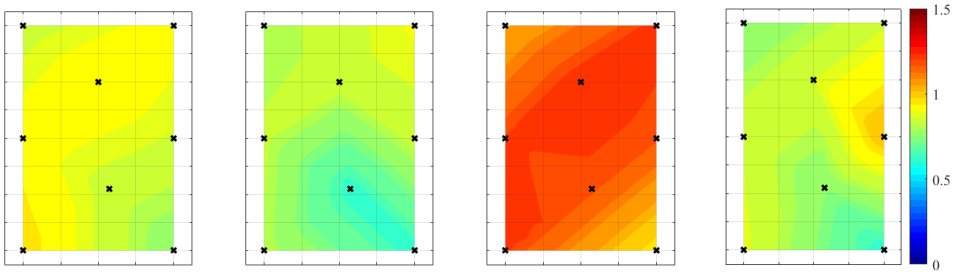

(**a**) Near-surface turbine (**b**) Near-bed turbine (**c**) Near-surface turbine (**d**) Near-bed turbine

Figure 19. Spatial variation in normalised damage equivalent loads from the root bending moment, as determined for (**a**,**b**) from the Telemac RANS model and (**c**,**d**) from the Telemac LES model, scale shown in (**d**) and is consistent across the figure, for the two turbine positions and the flood and ebb tides, across all operating flow speeds for a 5-year period, for the eight locations given in Figure 2 for the Telemac LES.

For both the Telemac RANS and Telemac LES variation in DELs, the time interval over which the conditions were extracted is consistent. This is the same as for the model conditions used in the LBM-LES comparison with the Telemac RANS at the nine extraction locations. The location of the extraction points is shown in Figure 2 and is included in the previous figures which show the spatial variation of DELs and highlight the smaller spatial area covered by these models. For the Telemac RANS model, the DEL variation is no greater than 12% across the site, consistent with the finding that the modelled bathymetry is consistent across the site; hence, there are similarities among the conditions. The near-surface has greater life time loads, which is consistent with the trend observed for the previous model comparison. Between the near-bed and near-surface turbine locations, the difference in predicted life time DELs is 28.5%. This highlights that understanding the conditions at a specific vertical position is important in understanding the life time. In comparison with the LBM-LES, there is limited information on the conditions across the range of U_{DA} to determine the 5-year through-life loading.

The average profiles and turbulence intensity values with disk-averaged velocity were used to calculate the load cycles for each set of conditions to determine the DELs. For a full comparison between the models and the measurement conditions, one location was chosen, namely the MU position, which was directly modelled by the Telemac RANS and is here considered sufficiently close to the Telemac LES to allow for nearest neighbour comparison. In addition, the mean turbulence intensity from the measurements was combined with the shear from the Telemac RANS model, following on from the single U_{DA} section. The difference with the predicted DEL from the measurement is shown in Table 3.

Table 3. Differences in the predicted damage equivalent loads for the 5-year lifespan between the measurement data and various model conditions, at one measurement location (NH1).

Type of Model	Near Surface	Near Bed
Telemac RANS (shear and TI)	−30.8%	−32.1%
Telemac RANS (shear) with measured TI	−2.7%	−2.9%
Telemac LES (shear and TI)	−8.1%	−16.1%

The differences in Table 3 show that, use of the Telemac LES model can provide through-life fatigue loads, it can get to within 8% for the near-surface turbine, but only within 16% for the near-bed turbine. This underestimation can be largely attributed to the reduced turbulence intensity predicted for the Telemac LES case, with the overall predictions being at least 4% lower in intensity at the measurement location across both tides and vertical positions, with differences in shear also contributing to the larger variation near the bed. Using the Telemac RANS only to predict the loads, these are between 31% and 32% for the near-surface and near-bed turbines, respectively. Which reflects the previously established difference in loads for the single U_{DA} case for the near-bed turbine in the flood tide, which had a 32% difference. Applying the larger variations in loads found for the near-surface turbine across the range of U_{DA} values resulted in a smaller variation in load prediction. However, the best prediction was found by combining the shear profiles from the Telemac RANS with the measured TI predictions, which provided loads within 3% to those predicted using the fully measured conditions. TIn general there is greater confidence in the loading predictions for the near-bed turbine being representative of the influence of real-site conditions compared to the near-surface predictions. This is due to the inherent limitations with ADCPs [31,49], with the intensity values for the near-surface turbine more likely to be affected by the interference between waves and turbulence kinematics and the greater distance in the plan area between the ADCP beams.

6. Discussion

The three concurrent ADCP deployments analysed in this study represent a unique dataset within one of the major tidal stream sites in Europe and in close proximity to areas at which turbine deployment is currently planned by two developers: Normandie Hydrolienne and Hydroquest. Whilst there are recognised limitations to ADCP measurements, [28,29], for inferring turbulence characteristics, the high sampling frequency employed and the use of a central fifth beam on one device for wave measurement maximises the data quality for the analysis of both turbulence characteristics and turbulence co-existing with surface waves. The analysis and model predication of the flow conditions focused on the characterisation of the flow over a range of disc-averaged velocities, as defined by the IEC standard, for a representative turbine diameter and two representative hub depths. Between the measurement devices, separated by 59.7–145.3 m, the occurrence of disc-averaged velocity is comparable, although small differences are observed in the shear across the rotor plane and magnitude of the turbulence intensity. This variation in turbulence intensity is greater for the near-surface turbine than the near-bed turbine, which is expected to be partly due to the greater uncertainty in ADCP measurement and the influence of waves over this depth range. Aggregated damage equivalent loads based on the measurements only for a single design case have greater variation at the near-surface location by up to 15%.

Damage equivalent loads have been predicted by the application of a blade element model to a range of disc-averaged velocities with the onset flow modelled based on the corresponding shear profiles superposed with a time-varying velocity field defined by a von Kármàn spectral model assuming frozen turbulence. This approach is similar to other blade element implementations, which has been shown to provide agreement with unsteady loads at the experimental scale [10], and is computationally efficient. Whilst a range of alternative techniques are available [47,54], this provides a consistent basis to

assess the impact of the differing measurements and predictions of unsteady conditions. This approach does, however involve a number of simplifications, particularly with regard to turbine operation and the onset flow. In particular, the turbine operation is based on a single tip speed ratio only. As such, the impact of power capping to limit rotor thrust is not captured. This would be expected to reduce the thrust loading, and hence root bending in the flow speeds above the rated speeds. Similarly, mechanisms such as pitch control, which may be utilised to realise power-capping, would also be expected to mitigate loads. However, herein, a fixed pitch and a fixed operating point have been considered throughout to quantify the impact of flow characteristics on a single measure of fatigue loading.

To assess through-life loads, unsteady loads are predicted for the full range of disc-averaged velocity increments. To simplify this stage of the analysis, loads were obtained for the averaged flow conditions within each flow speed bin and this is combined with the flow speed occurrence to obtain long-term loading. This follows the approach of Veers [55] and provides a consistent approach to compare between alternative predictions and measurements. When the model through-life loading predictions are compared to the measurements, they underestimate the loads by 30–32% for the Telemac RANS and by 8–16% for the Telemac LES. When the measured turbulence intensity is applied to the Telemac RANS shear conditions, the loads are within 3% for both the near-bed and near-surface turbines. The load predictions across the range of conditions are heavily influenced by the chosen turbulence properties. The near-surface turbine experiences greater through-life loading than the near-bed turbine, using both models and measurement data. This differs from the trend observed for a single flow speed bin due to the higher values of disc-averaged velocity that occur at the near-surface location. All models provide insights into the spatial variation of turbine exposure to fatigue loads over a much wider area than the ADCP deployments. There is much greater spatial variation of up to 39% for LES-based models than the 30% for RANS across the 1.6 km by 0.8 km region of the modelled site.

The through-life loading for the LBM-LES model is not shown here as, due to the computational cost, only the flood and ebb conditions at a single flow speed increment were extracted at each location that cannot be used to infer conditions across the range of operating velocities. Ideally, multiple samples would be extracted to allow a prediction of turbulence characteristics and hence through-life loading. The impact of waves on fatigue loading was also not analysed at this stage, although an initial comparison of the occurrence of wave conditions at the site from the measurements and Delft3D model was shown. Various methods have been developed to assess the impact of waves on turbulence characteristics and fatigue loads and an initial assessment of the impact of waves on the magnitude of measured turbulence intensity, and the impact on turbine loads, is given in [32].

An additional parameter which is considered when evaluating fatigue loads is the damage fraction, given by Palmgren miner's rule [45,56]. To place the DEL findings in context the variation of load cycles at each U_{DA}, combined with the maximum loads experienced, the total damage fraction is determined. For a period of 5 years, the total damage should not exceed 1 to avoid fatigue failure. Across all models and measurements, the predicted loading experienced on the near-bed turbine results in a damage fraction of less than 1, so failure will not occur without the need for a safety factor. For the near-surface turbine, considering only the loading from the Telemac RANS predictions for both the shear and turbulence, the blades would fail across half of the eight extraction locations, and therefore require a design safety factor of at least 2.1 for no failure to occur based on the predicted loads.

7. Conclusions

The design of tidal stream turbines requires the prediction of fatigue loading through the operating life. This requires understanding the occurrence and magnitude of mean velocity, velocity shear, and unsteady velocities due to turbulence and waves. A unique set of three current ADCP measurements and predictions obtained with several models

are analysed to assess the occurrence and spatial variation of the flow characteristics that influence turbine fatigue loading across a region of one of the major tidal stream sites in European waters, Raz Blanchard. Between the ADCPs, separated by 53–145 m, the occurrence of disc-averaged velocities is equivalent. Between the measurement locations, the velocity shear across the vertical extent of the rotor varies by 18–22%. The variation in the turbulence intensity with flow speed follows a similar trend for all locations, reducing with flow speed and typically greater on the flood tide than the ebb. This disparity is greater for a near-bed turbine location (14.2% flood, 12.4% ebb for flow speeds above 2 m/s) than a near-surface turbine location (11.7% flood, 11.3% ebb). The predictions of velocity, shear, and turbulence with three resource models provides insights into both prediction accuracy and the spatial variation of the flow over a wider region of the site, approximately 1.6 km by 0.8 km. This includes two different implementations of the Telemac model with the finest horizontal resolution of 5 m and a two-equation RANS model and LES used for turbulence closure, and an LBM-LES model in which bathymetry was resolved to within 0.25 m. Telemac RANS provides shear over the rotor plane of a similar magnitude to the ADCP measurements but underestimates the measured turbulence at the same locations. The Telemac LES predicts slightly higher values for turbulence intensity than the Telemac RANS and the LES-LBM predicts lower values at most locations. Each model also predicts a significant variation in turbulence intensity across the region of the studied site, with the magnitude and spatial variation differing between flood- and ebb-tides and with greater spatial variation observed for a near-bed turbine location.

To assess the impact of the predicted spatial variation of shear and turbulence on turbine design, damage equivalent loads are evaluated using an unsteady blade element momentum theory model with an unsteady inflow defined by measured—and modelled—conditions. The use of both shear and turbulence predicted by Telemac RANS underestimates fatigue loads by 32% for a near-bed turbine and 40% for a near-surface turbine relative to the use of the shear and turbulence measured at the ADCP locations. This disparity largely follows from the under-prediction of the turbulence intensity and reduces to between 1% and 10% for the near-bed and near-surface turbine locations, respectively, if the onset flow is modelled using predicted shear and measured turbulence. In comparison, there is 3% or 8% variation in the through-life DEL directly obtained using the data from the three ADCPS for a near-bed or near-surface location. The Telemac LES and LES-LBM models also underestimate turbulence relative to measurement but the different spatial variation of shear and turbulence intensity across the rotor plane result in different spatial variations of fatigue loading across the site. Throughout this study, the measured turbulence intensity is based on the fluctuating velocity measured using ADCPs. However, it is known that the measured fluctuations will actually include both turbulence and wave-induced kinematics and so the turbulence intensity may be expected to be lower than reported. Measurements indicate that irregular waves occur at this site with mean values of significant wave height ranging from 1 to 1.5 m and wave periods ranging from 8 to 10 s occurring over a range of flow speeds. Delft3D is shown to provide a reasonable prediction of the occurrence and mean of the wave height but with a greater disparity in the wave period over the measured period. At this stage, no attempt has been made to account for the influence of wave-induced kinematics on the calculated turbulence intensity or on the resulting fatigue loads; this is the subject of further study.

Author Contributions: Conceptualisation, H.M. and T.S.; Data curation, H.M., J.T., P.M., J.H., and E. M.; Formal analysis, H.M.; Funding acquisition, S.G., P.T., and T.S.; Investigation, H.M.; Methodology, H.M. and T.S.; Project administration, T.S.; Software, J.T., S.G., P.M., J.H., and E.M.; Supervision, S.G., P.T., and T.S.; Writing—original draft, H.M.; Writing—review and editing, H.M., S.D., and T.S. All authors have read and agreed to the published version of the manuscript.

Funding: This research was funded by Tidal Stream Industry Energiser project (TIGER), co-financed by the European Regional Development Fund through the INTERREG France (Channel) England Programme: Interreg VA.

Data Availability Statement: Measured ADCP data were gathered during the Interreg TIGER project. Further information on the deployment campaigns and underlying ADCP data can be found in T1.7.3 (https://interregtiger.com/download/tiger-tidal-test-procedure-reports/, accessed on 26 June 2023). Overview of models used is given in [36]. Underlying model data are provided in the references given. Variation in the flow properties with disk-averaged velocity as reported in this study and employed for fatigue load analysis is available from https://doi.org/10.48420/24236593 (accessed on 28 September 2023). We are grateful to the French navy SHOM ("Service Hydrographique et Océanographique de la Marine") for providing access to bathymetric data (http://data.shom.fr/, accessed on 6 June 2023).

Acknowledgments: This work was supported by the Tidal Stream Industry Energiser project (TIGER), co-financed by the European Regional Development Fund through the INTERREG France (Channel) England Programme: Interreg VA.

Conflicts of Interest: The authors declare no conflict of interest.

References

1. Coles, D.; Angeloudis, A.; Greaves, D.; Hastie, G.; Lewis, M.; MacKie, L.; McNaughton, J.; Miles, J.; Neill, S.; Piggott, M.; et al. A review of the UK and British Channel Islands practical tidal stream energy resource. *Proc. R. Soc. Math. Phys. Eng. Sci.* **2021**, *477*, 20210469. [CrossRef]
2. Afgan, I.; McNaughton, J.; Rolfo, S.; Apsley, D.; Stallard, T.; Stansby, P. Turbulent flow and loading on a tidal stream turbine by LES and RANS. *Int. J. Heat Fluid Flow* **2013**, *43*, 96–108. [CrossRef]
3. Ahmed, U.; Apsley, D.; Afgan, I.; Stallard, T.; Stansby, P.K. Fluctuating Loads on a Tidal Turbine Due to Velocity Shear and Turbulence: Comparison of CFD with Field Data. *Renew. Energy* **2017**, *112*, 235–246. [CrossRef]
4. Apsley, D.D.; Stallard, T.; Stansby, P.K. Actuator-line CFD modelling of tidal-stream turbines in arrays. *J. Ocean. Eng. Mar. Energy* **2018**, *4*, 259–271. [CrossRef]
5. Ouro, P.; Harrold, M.; Stoesser, T.; Bromley, P. Hydrodynamic loadings on a horizontal axis tidal turbine prototype. *J. Fluids Struct.* **2017**, *71*, 78–95. [CrossRef]
6. Olczak, A.; Stallard, T.; Feng, T.; Stansby, P.K. Comparison of a RANS blade element model for tidal turbine arrays with laboratory scale measurements of wake velocity and rotor thrust. *J. Fluids Struct.* **2016**, *64*, 87–106. [CrossRef]
7. McCann, G.N.; Hitchcock, S.; Lane, S. Implications of Site-Specific Conditions on the Prediction of Loading and Power Performance of a Tidal Stream Device. In Proceedings of the 2nd International Conference of Ocean Energy (ICOE 2008), Brest, France, 15–17 October 2008; pp. 1–9.
8. Masters, I.; Chapman, J.C.; Willis, M.R.; Orme, J.A.C. A robust Blade Element Momentum Theory model for tidal stream turbines including tip and hub loss corrections. *Proc. Inst. Mar. Eng. Sci. Technol. Part J. Mar. Eng. Technol.* **2011**, *10*, 25–35. [CrossRef]
9. Perez, L.; Cossu, R.; Grinham, A.; Penesis, I. An investigation of tidal turbine performance and loads under various turbulence conditions using Blade Element Momentum theory and high-frequency field data acquired in two prospective tidal energy sites in Australia. *Renew. Energy* **2022**, *201*, 928–937. [CrossRef]
10. Mullings, H.; Stallard, T. Analysis of tidal turbine blade loading due to blade scale flow. *J. Fluids Struct.* **2022**, *114*, 103698. [CrossRef]
11. Mullings, H.; Stallard, T. Assessment of dependency of unsteady onset flow and resultant tidal turbine fatigue loads on measurement position at a tidal site. *Energies* **2021**, *14*, 5470. [CrossRef]
12. Thiébaut, M.; Filipot, J.F.; Maisondieu, C.; Damblans, G.; Duarte, R.; Droniou, E.; Chaplain, N.; Guillou, S. A comprehensive assessment of turbulence at a tidal-stream energy site influenced by wind-generated ocean waves. *Energy* **2020**, *191*, 116550. [CrossRef]
13. Mercier, P.; Guillou, S.S.; Thiébot, J.; Poizot, E. Turbulence characterisation during ebbing and flooding tides in the Raz Blanchard with large eddy simulations. In Proceedings of the 14th European Wave and Tidal Energy Conference, Plymouth, UK, 5–9 September 2021.
14. Furgerot, L.; Sentchev, A.; Bailly du Bois, P.; Lopez, G.; Morillon, M.; Poizot, E.; Méar, Y.; Bennis, A.C. One year of measurements in Alderney Race: preliminary results from database analysis. *Philos. Trans. Ser. Math. Phys. Eng. Sci.* **2020**, *378*, 20190625. [CrossRef] [PubMed]
15. Guillou, N.; Neill, S.P.; Thiébot, J. Spatio-temporal variability of tidal-stream energy in north-western Europe. *Philos. Trans. R. Soc. Math. Phys. Eng. Sci.* **2020**, *378*, 20190493. [CrossRef] [PubMed]
16. Guillou, S.; Bourgoin, A.; Thiébot, J.; Ata, R. On the spatial variability of the flow characteristics at a Tidal energy site : Case of the Raz Blanchard. In Proceedings of the 14th European Wave and Tidal Energy Conference, Plymouth, UK, 5–9 September 2021; pp. 1–8.
17. Mercier, P.; Grondeau, M.; Guillou, S.; Thiébot, J.; Poizot, E. Numerical study of the turbulent eddies generated by the seabed roughness. Case study at a tidal power site. *Appl. Ocean. Res.* **2020**, *97*, 102082. [CrossRef]
18. Mercier, P.; Guillou, S. The impact of the seabed morphology on turbulence generation in a strong tidal stream. *Phys. Fluids* **2021**, *33*, 055125. [CrossRef]

19. Bennis, A.C.; Furgerot, L.; Bailly Du Bois, P.; Dumas, F.; Odaka, T.; Lathuilière, C.; Filipot, J.F. Numerical modelling of three-dimensional wave-current interactions in complex environment: Application to Alderney Race. *Appl. Ocean. Res.* **2020**, *95*, 102021. [CrossRef]
20. Hardwick, J.; Mackay, E.B.; Ashton, I.G.; Smith, H.C.; Thies, P.R. Quantifying the effects of wave—current interactions on tidal energy resource at sites in the english channel using coupled numerical simulations. *Energies* **2021**, *14*, 3625. [CrossRef]
21. Mackay, E.; Hardwick, J.; Coles, D.; Mercier, P.; Guillou, S.; Pinon, G.; Sedrati, M.; Mullings, H; Stallard, T; Ouro, P; et al. Consolidated Report on Site and Turbine Modelling. Technical Report. 2023. Available online: https://interregtiger.com/download/tiger-report-consolidated-report-on-site-and-turbine-modelling/ (accessed on 20 January 2023).
22. Mullings, H.R.; Stallard, T. Assessment of tidal turbine load cycles using synthesised load spectra, including blade-scale fluctuations. In Proceedings of the 13th European Wave and Tidal Energy Conference, Naples, Italy, 1–6 September 2019; pp. 1–9.
23. Jakovljevi, A.; Paboeuf, S.; Dias, F. Impact of wave-current interactions on tidal current turbine performance in storm conditions. In Proceedings of the 12th European Wave and Tidal Energy Conference, Cork, Ireland, 27 August–2 September 2017; pp. 1–9.
24. Bourgoin, A.C.; Guillou, S.S.; Thiébot, J.; Ata, R. Turbulence characterization at a tidal energy site using large-eddy simulations: case of the Alderney Race. *Philos. Trans. Ser. Math. Phys. Eng. Sci.* **2020**, *378*, 20190499. [CrossRef] [PubMed]
25. Thiébaut, M.; Sentchev, A.; Bailly du Bois, P. Monitoring tidal currents with a towed adcp at tidal energy site in alderney race (Raz blanchard). In *Advances in Renewable Energies Offshore, Proceedings of the 3rd International Conference on Renewable Energies Offshore, RENEW 2018, Lisbon, Portugal, 8–10 October 2018*; CRC Press: Boca Raton, FL, USA, 2018; pp. 49–56.
26. Sentchev, A.; Nguyen, T.D.; Furgerot, L.; Bailly du Bois, P. Underway velocity measurements in the Alderney Race: towards a three-dimensional representation of tidal motions. *Philos. Trans. Ser. Math. Phys. Eng. Sci.* **2020**, *378*, 20190491. [CrossRef] [PubMed]
27. ORE Catapult TIGER Site Development Report: The Raz Blanchard T3.2.1. Technical Report. June 2023. Available online: https://interregtiger.com/download/site-development-report-raz-blanchard/ (accessed on 4 July 2023).
28. Guion, R.U.G.; Young, A.M. The Frequency Response of Acoustic Doppler Current Profilers Spatiotemporal response and implications for tidal turbine site assessment. In Proceedings of the Oceans 2014 St. John's, NL, Canada, 14–19 September 2014; pp. 1–10.
29. Young, A.M.; Atkins, N.R.; Clark, C.J.; Germain, G. An Unsteady Pressure Probe for the Measurement of Flow Unsteadiness in Tidal Channels. *IEEE J. Ocean. Eng.* **2019**, *45*, 1411–1426. [CrossRef]
30. Togneri, M.; Masters, I.; Fairley, I. Wave-turbulence separation at a tidal energy site with empirical orthogonal function analysis. *Ocean Eng.* **2021**, *237*, 109523. [CrossRef]
31. Perez, L.; Cossu, R.; Grinham, A.; Penesis, I. Evaluation of wave-turbulence decomposition methods applied to experimental wave and grid-generated turbulence data. *Ocean Eng.* **2020**, *218*, 108186. [CrossRef]
32. Mullings, H.; Draycott, S.; Stallard, T. Turbine fatigue load prediction from field measurements of waves and turbulence. In Proceedings of the Proceedings of 15th European Wave and Tidal Energy Conference, Bilbao, Spain, 3–7 September 2023; pp. 3–7. [CrossRef]
33. Thiébot, J.; Guillou, N.; Guillou, S.; Good, A.; Lewis, M. Wake field study of tidal turbines under realistic flow conditions. *Renew. Energy* **2020**, *151*, 1196–1208. [CrossRef]
34. Thiebot, J.; Bailly du Bois, P.; Guillou, S. Numerical modeling of the effect of tidal stream turbines on the hydrodynamics and the sediment transport-Application to the Alderney Race (Raz Blanchard). *Renew. Energy* **2015**, *75*, 356–365. [CrossRef]
35. Mercier, P.; Grondeau, M.; Guillou, S.; Thiébot, J.; Poizot, E. Towards the modelling of turbulence at tidal stream power sites with the Lattice Boltzmann Method. In Proceedings of the 12th European Wave and Tidal Energy Conference, Cork, Ireland, 27 August–1 September 2017; pp. 1–8.
36. Mackay, E.; Hardwick, J.; Thies, P.; Mercier, P.; Grondeau, M.; Guillou, S.; Coles, D.; Pinon, G.; Sedrati, M.; Ouro, P.; et al. Overview of resource and turbine modelling in the Tidal Stream Industry Energiser Project: TIGER. In Proceedings of the Proceedings of the 15th European Wave and Tidal Energy Conference, Bilbao, Spain, 3–7 September 2023; pp. 3–7. [CrossRef]
37. Milne, I.A.; Sharma, R.N.; Flay, R.G.J.; Bickerton, S. The Role of Waves on Tidal Turbine Unsteady Blade Loading. In Proceedings of the 3rd International Conference on Ocean Energy, Bilbao, Spain, 2–5 September 2010; pp. 1–6.
38. Parkinson, S.G.; Collier, W.J. Model validation of hydrodynamic loads and performance of a full-scale tidal turbine using Tidal Bladed. *Int. J. Mar. Energy* **2016**, *16*, 279–297. [CrossRef]
39. Downing, S.D.; Socie, D.F. Simple rainflow counting algorithms. *Int. J. Fatigue* **1982**, *4*, 31–40. [CrossRef]
40. Endo, T.; Mitsunaga, K.; Takahashi, K.; Kobayashi, K.; Matsuishi, M. Damage evaluation of metals for random or varying loading—three aspects of rain flow method. *Mech. Behav. Mater.* **1974**, *1–2*, 371–380.
41. Weller, S.D.; Thies, P.R.; Gordelier, T.; Johanning, L. Reducing Reliability Uncertainties for Marine Renewable Energy. *J. Mar. Sci. Eng.* **2015**, *3*, 1349–1361. [CrossRef]
42. Gretton, G.I. *PerAWaT—Development of a Computational Fluid Dynamics Model for a Horizontal Axis Tidal Current Turbine WG3 WP5 D1*; Technical Report; ETI: Loughborough, UK, 2010. [CrossRef]
43. Scarlett, G.T.; Sellar, B.; van den Bremer, T.; Viola, I.M. Unsteady hydrodynamics of a full-scale tidal turbine operating in large wave conditions. *Renew. Energy* **2019**, *143*, 199–213. [CrossRef]

44. Ouro, P.; Mullings, H.; Stallard, T. Establishing confidence in predictions of fatigue loading for floating tidal turbines based on large-eddy simulations and unsteady blade element momentum. In Proceedings of the Trends in Renewable Energies Offshore, Lisbon, Portugal, 11 September 2023; pp. 915–924. [CrossRef]
45. Veers, P. *Three-Dimensional Wind Simulation*; Technical Report; Sandia National Laboratories: Sandia, CA, USA, 1988.
46. Milne, I.a.; Day, a.H.; Sharma, R.N.; Flay, R.G. Blade loads on tidal turbines in planar oscillatory flow. *Ocean Eng.* **2013**, *60*, 163–174. [CrossRef]
47. Togneri, M.; Pinon, G.; Carlier, C.; Choma Bex, C.; Masters, I. Comparison of synthetic turbulence approaches for blade element momentum theory prediction of tidal turbine performance and loads. *Renew. Energy* **2020**, *145*, 408–418. [CrossRef]
48. Taylor, G.I. Turbulence in a contracting stream. *ZAMM-J. Appl. Math. Mech. Angew. Math. Mech.* **1935**, *15*, 91–96. [CrossRef]
49. Togneri, M.; Masters, I.; Carlier, C.; Choma Bex, C.; Pinon, G. Comparison of synthetic turbulence approaches for two numerical tidal turbine models. In Proceedings of the 12th European Wave and Tidal Energy Conference, Cork, UK, 27 August–1 September 2017; pp. 1–10.
50. Jarrin, N.; Benhamadouche, S.; Laurence, D.; Prosser, R. A synthetic-eddy-method for generating inflow conditions for large-eddy simulations. *Int. J. Heat Fluid Flow* **2006**, *27*, 585–593. [CrossRef]
51. DNV-GL. *DNV GL STANDARD: Tidal Turbines*; Technical Report; DNV GL: Oslo, Norway, 2015.
52. IEC. *Power Performance Assessment of Electricity Producing Tidal Energy Converters, IEC 62600-200*; Technical Report; International Electrotechnical Commission: Geneva, Switzerland, 2012.
53. Mercier, P.; Guillou, S.S. Tracking a large vortex at a tidal power site. In Proceedings of the 15th European Wave and Tidal Energy Conference, Bilbao, Spain, 3–7 September 2023. [CrossRef]
54. Choma Bex, C.; Carlier, C.; Fur, A.; Pinon, G.; Germain, G.; Rivoalen, É. A stochastic method to account for the ambient turbulence in Lagrangian Vortex computations. *Appl. Math. Model.* **2020**, *88*, 38–54. [CrossRef]
55. Veers, P. *Fatigue Loading of Wind Turbines*; Woodhead Publishing Limited: Sawston, UK, 2009; pp. 130–158. [CrossRef]
56. Mullings, H.R.; Stallard, T.J.; Payne, G.S. Operational Loads on a Tidal Turbine due to Environmental Conditions. In Proceedings of the 27th International Offshore and Polar Engineering Conference, San Francisco, CA, USA, 25–30 June 2017; pp. 1–14.